



HAL
open science

Cobalt(II) coordination complex with 2,5-bis(pyridine-2-yl)-1,3,4-thiadiazole and thiocyanate as co-ligand: Synthesis, crystal structure, Hirshfeld surface analysis, spectroscopic, thermal and magnetic properties

Abdelhakim Laachir, Ferdaousse Rhoufal, Salaheddine Guesmi, El Mostafa Ketatni, Laurent Jouffret, El-Kebir Hlil, Nicolas Sergent, Saïd Obbade, Fouad Bentiss

► To cite this version:

Abdelhakim Laachir, Ferdaousse Rhoufal, Salaheddine Guesmi, El Mostafa Ketatni, Laurent Jouffret, et al.. Cobalt(II) coordination complex with 2,5-bis(pyridine-2-yl)-1,3,4-thiadiazole and thiocyanate as co-ligand: Synthesis, crystal structure, Hirshfeld surface analysis, spectroscopic, thermal and magnetic properties. *Journal of Molecular Structure*, 2020, 1208, pp.127892. 10.1016/j.molstruc.2020.127892 . hal-02492465

HAL Id: hal-02492465

<https://hal.science/hal-02492465>

Submitted on 15 Dec 2020

HAL is a multi-disciplinary open access archive for the deposit and dissemination of scientific research documents, whether they are published or not. The documents may come from teaching and research institutions in France or abroad, or from public or private research centers.

L'archive ouverte pluridisciplinaire **HAL**, est destinée au dépôt et à la diffusion de documents scientifiques de niveau recherche, publiés ou non, émanant des établissements d'enseignement et de recherche français ou étrangers, des laboratoires publics ou privés.

Cobalt(II) coordination complex with 2,5-bis(pyridine-2-yl)-1,3,4-thiadiazole and thiocyanate as co-ligand: Synthesis, crystal structure, Hirshfeld surface analysis, spectroscopic and magnetic properties

Abdelhakim Laachir ^{a,b}, Ferdaousse Rhoufal ^{a,b}, Salaheddine Guesmi ^a, El Mostafa Ketatni ^c, Laurent Jouffret ^d, El Kebir Hlil ^e, Nicolas Sergent ^f, Saïd Obbade ^{f,*}, Fouad Bentiss ^{b,*},

^a *Laboratory of Coordination and Analytical Chemistry (LCCA), Faculty of Sciences, Chouaib Doukkali University, PO Box 20, M-24000 El Jadida, Morocco*

^b *Laboratory of Catalysis and Corrosion of Materials (LCCM), Faculty of Sciences, Chouaib Doukkali University, PO Box 20, M-24000 El Jadida, Morocco*

^c *Laboratory of Organic and Analytical Chemistry, Faculty of Science and Technology, University Sultan Moulay Slimane, PO Box 523, Beni-Mellal, Morocco*

^d *Institut de Chimie de Clermont-Ferrand, CNRS, Université Clermont Auvergne, SIGMA Clermont, F-63000 Clermont-Ferrand, France*

^e *Institut Néel, CNRS et Université Grenoble Alpes, BP 166, 38042 Grenoble, France*

^f *Univ. Grenoble Alpes, Univ. Savoie Mont Blanc, CNRS, Grenoble INP, LEPMI, 38000 Grenoble, France*

* Corresponding author.
said.obbade@phelma.grenoble-inp.fr
fbentiss@gmail.com

ABSTRACT

The bis(2,5-di(pyridin-2-yl)-1,3,4-thiadiazole- κ^2N,N')-bis(thiocyanato- κ^1N)cobalt(II) complex has been synthesized from the reaction of 2,5-bis(pyridin-2-yl)-1,3,4-thiadiazole (L) with metallic salt $\text{CoCl}_2 \cdot 6\text{H}_2\text{O}$ and thiocyanate ion (SCN^-) as coligand in $\text{H}_2\text{O}/\text{CH}_3\text{CN}$ at room temperature. The synthesized complex ($\text{CoL}_2(\text{SCN})_2$) has been fully characterized by single crystal X-ray diffraction, Hirshfeld surface analysis, as well as UV-Visible, FTIR, Raman, and NMR spectroscopy. TGA analysis and magnetic measurements were also performed. $\text{CoL}_2(\text{SCN})_2$ crystallizes in monoclinic symmetry and $P 2_1/c$ space group with two independent cobalt crystallographic sites, where each cobalt atom is localized in a distorted octahedral environment CoN_6 , with the thiadiazole molecules (L) as bidentate ligands in equatorial sites and terminal SCN^- ions in axial positions. The crystal cohesion is assured by intermolecular hydrogen bonding, $\text{C}-\text{H} \cdots \pi$ and $\pi-\pi$ stacking; in addition to the N–Cu coordination bonds. This has been confirmed by the three dimensional Hirshfeld surface analysis and the two dimensional fingerprint plots that highlight the dominance of intermolecular interactions $\text{C} \cdots \text{H}/\text{H} \cdots \text{C}$ and $\text{S} \cdots \text{H}/\text{H} \cdots \text{S}$. The thermal analysis of $\text{CoL}_2(\text{SCN})_2$ reveals that this complex is thermally stable up to 200 °C. Variable-temperature magnetic susceptibility measurements on $\text{CoL}_2(\text{SCN})_2$ complex indicated an antiferromagnetic exchange between the two non-equivalent cobalt(II) ions with a ferrimagnetic behaviour.

Keywords: 2,5-Bis(pyridin-2-yl)-1,3,4-thiadiazole; Thiocyanate; Mononuclear Co(II) complex; Crystal structure; Hydrogen bonds; Antiferromagnetic interaction.

1. Introduction

Over the last few decades several research studies have shown the importance of transition metal complexes in various fields such as biology for their antibacterial [1,2], antifungal [1,3] or antitumor [4,5] activities; pharmacology for the treatment of certain diseases [6,7] and catalysis for the selectivity of reactions [8,9]. Since the nitrogen atom is present in many natural molecules or in those of pharmacological interest [6,10], research has been devoted to the synthesis of transition metal complexes with hetero-atom and chelating ligands [11-13]. It is also well established that some of these organic molecules (drugs) are much more effective when administered linked to a metal [14-16]. The 1,3,4-thiadiazole derivatives such as 2,5-bis(pyridin-2-yl)-1,3,4-thiadiazole (L) have been studied and have allowed access essentially to mono and bimetallic complexes [17-22]. The biological activity of some of these complexes was examined: It confirms the growth of the efficiency of the ligand according to its environment in the coordination sphere of the metal. For example, in phytopathology, we have shown that this efficiency varies according to the following sequence: $\text{NiL}_2(\text{N}_3)_2 > \text{Ni}_2\text{L}_2(\text{H}_2\text{O})_4\text{Cl}_4 \cdot 3\text{H}_2\text{O} > \text{L}$ [23,24]. Recently, we have reported the synthesis of mono and binuclear compounds of transition metals (M = Cu, Ni and Co) with pseudo halide anions (N_3^- and SCN^-) as co-ligands [23-28]. The magnetic study of μ_2 -1,1-azido double-bridged $[\text{Cu}_2\text{L}_2(\mu\text{-N}_3)_2(\text{N}_3)_2]$ complex revealed that the latter is weakly antiferromagnetic [27].

The pseudo halide complexes so exhibit interesting properties in many areas, this prompted us to continue this study by trying to isolate other complexes with Co(II) metal, 2,5-bis(pyridin-2-yl)-1,3,4-thiadiazole ligand (L) and thiocyanate ions. Recently, the new complex of formula $(\text{C}_{26}\text{H}_{16}\text{CoN}_{10}\text{S}_4)$ noted $\text{CoL}_2(\text{SCN})_2$ has been synthesized under heating for 3 days and its crystallographic structure was briefly described by Wang [29]. In parallel and independently of this work, we synthesized the same complex but in mild thermal conditions (without heating) and herein we report a detailed structural study and Hirshfeld surface analysis of $\text{CoL}_2(\text{SCN})_2$ complex as well as its spectroscopic characterisations (IR, UV-Visible and Raman). The magnetic properties of the title complex were also performed and discussed.

2. Experimental

2.1. Materials

The ligand, namely 2,5-bis(pyridin-2-yl)-1,3,4-thiadiazole (L) was synthesized according to the literature procedure [30]. All solvents and reagents for synthesis were purchased from Aldrich and Merck and used as received without further recrystallization or distillation.

2.2. Synthesis of the title compound $Co(C_{12}H_8N_4S)_2(NCS)_2 : CoL_2(NCS)_2$

A mixture of ligand L (24 mg, 0.1 mmol) and CH_3CN (10 mL) was carefully layered onto a solution of $CoCl_2 \cdot 6H_2O$ (24 mg, 0.1 mmol) and $KSCN$ (20 mg, 0.2 mmol) in CH_3CN/H_2O (1:1 v/v, 10 mL). The test tube was sealed with parafilm and left to stand at room temperature. Slow diffusion between the metal salt solution and the 1,3,4-thiadiazole ligand (L) produced red block-shaped crystals of $CoL_2(NCS)_2$. They were separated, washed with cold ethanol and dried under vacuum. Yield: 55% (based on Co). Anal. Calcd. (%) for $C_{26}H_{16}CoN_{10}S_4$: C, 47.63; H, 2.46; N, 21.36; S, 19.56. Found (%): C, 47.69; H, 2.52; N, 21.29; S, 19.51; IR (KBr pellet, cm^{-1}): 2079 (vs), 1636 (m), 1600 (w), 1564 (w), 642 (w); UV-Vis (λ_{max} , nm (ϵ_{max} , $M^{-1} cm^{-1}$)) in DMSO solvent: 796 (860), 642 (180), 431 (2620), 317 (33720), 272 (27300).

2.3. Crystal X-ray data collection

Single crystal selected for the X-ray diffraction (XRD) data collection ($0.082 \times 0.084 \times 0.218$ mm) was mounted on cryoloop and tested on a Bruker APEX II diffractometer with a MoK_{α} graphite-monochromated radiation ($\lambda = 0.71073 \text{ \AA}$). The diffractometer is equipped with a CCD bidimensional detector and an OXFORD CRYOSTREAM 700 system to cool the sample to 173 K [31]. SAINT⁺ 6.02 program was used for extraction and integration of diffraction intensities [32] and SADABS program was carried out for correction of absorption effect [33]. The structures were solved by direct methods using SHELXL [34] and refined (by weighted full matrix least-square on

F^2 techniques) to convergence using the SHELXL program. All non-hydrogen atoms were refined anisotropically. All hydrogen atoms were positioned geometrically and refined using a riding model.

Routine powder X-ray diffraction (PXRD) data of pure phase for $\text{CoL}_2(\text{SCN})_2$ complex have been collected at room temperature in the angular range 5 to 70 of 2θ with a scan step width 0.016° using a X'pert Pro PANalytical $\theta/2\theta$ diffractometer (CuK_α radiation, $\lambda = 1.5405 \text{ \AA}$) in Bragg-Brentano geometry. Cell parameters have been refined using the pattern matching option of Fullprof suite [35,36], by means of PXRD profile patterns adjustment.

2.4. Hirshfeld surface analysis

The Hirshfeld surfaces calculated for $\text{CoL}_2(\text{NCS})_2$ complex provide additional information on the distinctive contributions made to the molecular packing by the independent molecules. Thus, a Hirshfeld surface analysis [37] and the associated two-dimensional fingerprint plots [38] were performed using CrystalExplorer17.5 [39] to figure out the normalized contact distance (d_{norm}), which depends on contact distances to the closest atoms outside (d_e) and inside (d_i) the surface. The 3D d_{norm} surfaces are mapped over a fixed colour scale of -0.185 to 1.334 and -0.222 to 1.337 a.u for $\text{Co(1)L}_2(\text{NCS})_2$ and $\text{Co(2)L}_2(\text{NCS})_2$ molecules respectively, and shape index mapped in the colour range of -1.0 to 1.0 a.u.

2.5. physical measurements

UV-Visible absorption spectra in dimethyl sulfoxide (DMSO) solvent were recorded in the range 200-900 nm using a SHIMADZU 2450 spectrophotometer. Element analyses (C, H, N and S) were performed on a VARIO-ELEMENTAR analyzer.

FTIR spectra were recorded on a SHIMADZU FT-IR 8400S spectrometer with samples dispersed in KBr pellets in the range $500\text{-}3000 \text{ cm}^{-1}$.

Raman spectra have been acquired with a Renishaw InVia spectrometer in micro-Raman configuration (objective $\times 50$) equipped with a Peltier cooled CCD detector. The 785 nm excitation line of a LASER diode have been used at a power less than 3 mW onto the sample in order to avoid local heating.

The ^1H and ^{13}C NMR spectra of complex were recorded with the Bruker AVANCE 300 at 25 °C. All chemical shifts ^1H and ^{13}C are given in ppm using dimethyl sulfoxide- d_6 (DMSO- d_6) DMSO as solvent.

Thermal gravimetric analysis (TGA) has been performed under air flow (20 ml/min), using a SETARAM TAG24-16 thermal analyzer and platinum crucibles, in the range of room temperature to 700°C under air with 5 °C min^{-1} fixed heating rate. The TGA curve has been normalized with respect to the sample weight.

Magnetic measurements were carried out using the commercial Physical Properties Measurements System device (Quantum Design, PPMS), and magnetization $M(T)$ was measured versus temperature ranging from 2 to 300 K, under an external magnetic field of 0.05 T. The magnetic field dependence of the magnetization $M(H)$ was also measured at 2 K by varying the applied magnetic field between -6 and 6 T.

3. Results and discussion

3.1. Crystal structure determination and description

The mononuclear title Co(II) complex, namely bis(2,5-di(pyridin-2-yl)-1,3,4-thiadiazole- κ^2N,N')-bis(thiocyanato- κ^1N)cobalt(II), $\text{Co}(\text{C}_{12}\text{H}_8\text{N}_4\text{S})_2(\text{NCS})_2$, was obtained by reaction between the thiadiazole ligand (L), $\text{CoCl}_2 \cdot \text{H}_2\text{O}$ and KSCN in $\text{H}_2\text{O}/\text{CH}_3\text{CN}$ solution. The obtained complex $\text{CoL}_2(\text{NCS})_2$, crystallizes in monoclinic symmetry and $P 2_1/c$ space group with two independent cobalt crystallographic sites, Co1 and Co2, and four $\text{CoL}_2(\text{SCN})_2$ molecules by unit cell as shown in Fig. 1. The details for the crystal data collection and the processing, together with the measurement parameters of the title complex are given in Table 1. Final atomic coordinates and isotropic or

equivalent isotropic displacement parameters are given in Table 2. The selected interatomic distances are listed in Table 3. Hydrogen bonds are reported in Table 4. CCDC 1878437 (CSD, Cambridge) contains the supplementary crystallographic information for the $\text{CoL}_2(\text{NCS})_2$ complex.

Crystal structure was solved in the centrosymmetric $P 2_1/c$ space group by means of a direct methods strategy that localizes the heavy atoms Co and S, followed by a Fourier-difference maps examination to localize non-hydrogen light atoms N and C. All non-hydrogen atoms were refined with anisotropic displacement factors. Hydrogen atoms were included in idealized position and refined with fixed isotropic displacement factors U_{eq} in the final cycles of refinement. The final refinement by using geometrical restraints with $\text{C-H} = 0.95 \text{ \AA}$ (aromatic ring). At the end of the crystal structure refinement a last Fourier-difference examination reveals no significant peak, with acceptable remaining maximum and minimum electron densities.

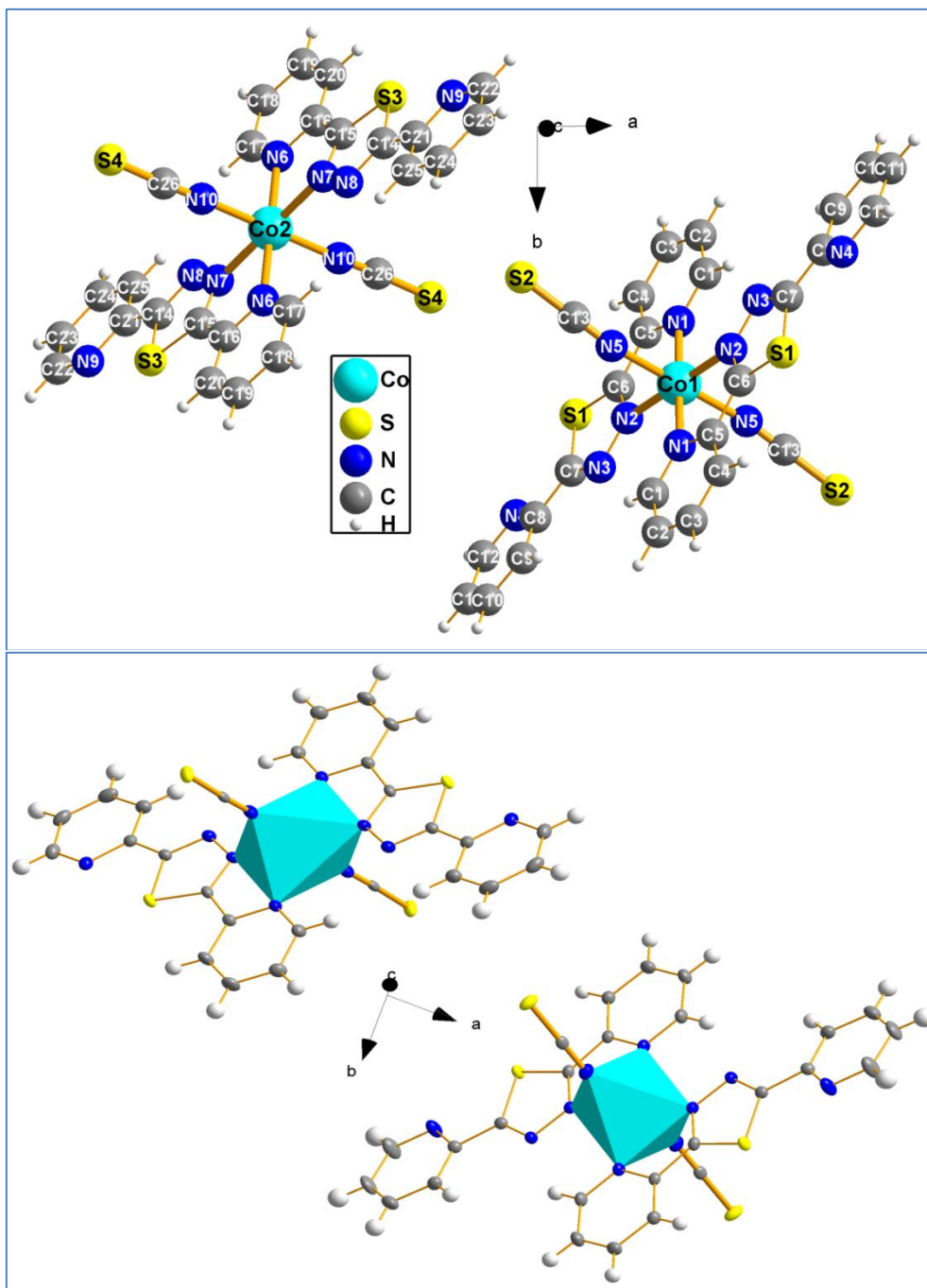


Fig. 1. Coordination environment cobalt sites in the crystal of $\text{CoL}_2(\text{NCS})_2$ complex.

Table 1Single crystal and structure refinement data for CoL₂(NCS)₂ complex.

Chemical formula	C ₂₆ H ₁₆ CoN ₁₀ S ₄	
Formula weight	655.66 g/mol	
Temperature	173(2) K	
Wavelength	0.71073 Å	
Crystal size	0.082 × 0.084 × 0.218 mm	
Crystal system	monoclinic	
Space group	<i>P</i> 2 ₁ / <i>c</i>	
Unit cell dimensions	<i>a</i> = 22.876(4) Å	<i>α</i> = 90°
	<i>b</i> = 7.9167(12) Å	<i>β</i> = 110.204(5)°
	<i>c</i> = 16.403(3) Å	<i>γ</i> = 90°
Volume	2787.8(8) Å ³	
Z	4	
Density (calculated)	1.562 g/cm ³	
Absorption coefficient	0.953 mm ⁻¹	
F(000)	1332	
Theta range for data collection	3.20 to 31.50°	
Index ranges	-33 ≤ <i>h</i> ≤ 33, -11 ≤ <i>k</i> ≤ 11, -24 ≤ <i>l</i> ≤ 23	
Reflections collected	105365	
Independent reflections	9198 [<i>R</i> _(int) = 0.0909]	
Coverage of independent reflections	99.0%	
Absorption correction	Numerical Mu From Formula	
Refinement method	Full-matrix least-squares on <i>F</i> ²	
Refinement program	SHELXL-2014/7 (Sheldrick, 2014)	
Function minimized	Σ <i>w</i> (<i>F</i> _o ² - <i>F</i> _c ²) ²	
Data / restraints / parameters	9198 / 0 / 373	
Goodness-of-fit on <i>F</i> ²	1.005	
Δ/ <i>σ</i> _{max}	0.002	
Final <i>R</i> indices	6184 data; <i>I</i> > 2 <i>σ</i> (<i>I</i>)	<i>R</i> ₁ = 0.0386, <i>wR</i> ₂ = 0.0719
	all data	<i>R</i> ₁ = 0.0808, <i>wR</i> ₂ = 0.0868
Weighting scheme	<i>W</i> = 1/[<i>σ</i> ² (<i>F</i> _o ²) + (0.0234 <i>P</i>) ² + 2.2054 <i>P</i>] where <i>P</i> = (<i>F</i> _o ² + 2 <i>F</i> _c ²)/3	
Largest diff. peak and hole	0.445 and -0.628 eÅ ⁻³	
R.M.S. deviation from mean	0.088 eÅ ⁻³	

Table 2

Fractional non hydrogen atomic coordinates and isotropic or equivalent isotropic displacement parameters (\AA^2).

	<i>x/a</i>	<i>y/b</i>	<i>z/c</i>	<i>U</i> _{eq}
Co1	0.0	0.5	0.0	0.01601(8)
Co2	0.5	0.0	0.0	0.01652(8)
S1	0.14339(2)	0.41758(6)	0.86879(3)	0.01936(10)
S2	0.16790(2)	0.82432(7)	0.19507(4)	0.02654(12)
S3	0.64515(2)	0.59909(6)	0.01490(3)	0.01983(10)
S4	0.33729(2)	0.79479(7)	0.74160(3)	0.02543(12)
N1	0.01138(7)	0.6963(2)	0.91514(10)	0.0178(3)
N2	0.06959(7)	0.3986(2)	0.95458(10)	0.0171(3)
N3	0.10123(7)	0.2480(2)	0.97058(10)	0.0176(3)
N4	0.21513(9)	0.1095(2)	0.87984(12)	0.0271(4)
N5	0.06951(8)	0.6134(2)	0.10116(11)	0.0228(4)
N6	0.49964(7)	0.7743(2)	0.07308(10)	0.0180(3)
N7	0.43210(7)	0.1561(2)	0.02660(10)	0.0181(3)
N8	0.39598(8)	0.1348(2)	0.07761(11)	0.0192(3)
N9	0.26665(7)	0.3951(2)	0.07693(11)	0.0200(3)
N10	0.42991(8)	0.9111(2)	0.89237(11)	0.0224(4)
C1	0.98090(9)	0.8441(3)	0.89676(13)	0.0209(4)
C2	0.99353(9)	0.9660(3)	0.84419(13)	0.0228(4)
C3	0.03935(9)	0.9342(3)	0.80875(13)	0.0209(4)
C4	0.07156(9)	0.7817(3)	0.82737(12)	0.0192(4)
C5	0.05611(8)	0.6663(2)	0.88000(12)	0.0165(4)
C6	0.08649(8)	0.5004(3)	0.90309(12)	0.0170(4)
C7	0.14161(9)	0.2409(2)	0.93041(12)	0.0167(4)
C8	0.18451(9)	0.0989(2)	0.93638(12)	0.0182(4)
C9	0.19257(9)	0.9699(3)	0.99661(13)	0.0227(4)
C10	0.23529(10)	0.8431(3)	0.99847(15)	0.0277(5)
C11	0.26679(11)	0.8506(3)	0.94057(15)	0.0321(5)
C12	0.25539(11)	0.9851(3)	0.88241(15)	0.0346(6)
C13	0.11056(9)	0.7013(3)	0.14001(12)	0.0184(4)
C14	0.35376(9)	0.2535(2)	0.06306(12)	0.0179(4)
C15	0.58300(9)	0.7099(2)	0.02373(12)	0.0178(4)
C16	0.54630(9)	0.6646(2)	0.07828(12)	0.0178(4)
C17	0.46242(9)	0.7377(3)	0.11827(13)	0.0210(4)
C18	0.46988(10)	0.5934(3)	0.16928(13)	0.0241(4)
C19	0.51813(10)	0.4839(3)	0.17473(14)	0.0261(5)
C20	0.55707(10)	0.5198(3)	0.12824(13)	0.0230(4)
C21	0.30817(9)	0.2697(2)	0.10731(13)	0.0186(4)
C22	0.22408(9)	0.4142(3)	0.11511(14)	0.0237(4)
C23	0.22112(10)	0.3133(3)	0.18268(14)	0.0263(5)
C24	0.26460(10)	0.1859(3)	0.21319(14)	0.0274(5)
C25	0.30960(10)	0.1624(3)	0.17502(13)	0.0239(4)
C26	0.39105(9)	0.8657(2)	0.82887(13)	0.0178(4)

Table 3Selected bond distances (Å) for the $\text{CoL}_2(\text{NCS})_2$ complex.

Co1–N5	2.0654(17)	Co2–N10	2.0563(17)
Co1–N2	2.1337(15)	Co2–N7	2.1442(16)
Co1–N1	2.1615(16)	Co2–N6	2.1529(16)
S1–C6	1.7164(18)	S1–C7	1.735(2)
S2–C13	1.633(2)	S3–C15	1.7188(19)
S3–C14	1.738(2)	S4–C26	1.631(2)
N1–C1	1.342(3)	N1–C5	1.358(2)
N2–C6	1.318(2)	N2–N3	1.373(2)
N3–C7	1.308(2)	N4–C12	1.339(3)
N4–C8	1.344(2)	N5–C13	1.166(3)
N6–C17	1.340(2)	N6–C16	1.356(2)
N7–C15	1.315(2)	N7–N8	1.374(2)
N8–C14	1.309(2)	N9–C22	1.336(2)
N9–C21	1.345(2)	N10–C26	1.168(3)
C1–C2	1.390(3)	C7–C8	1.473(3)
C2–C3	1.386(3)	C8–C9	1.388(3)
C3–C4	1.392(3)	C9–C10	1.394(3)
C4–C5	1.384(3)	C10–C11	1.378(3)
C5–C6	1.473(3)	C11–C12	1.393(3)
C14–C21	1.468(3)	C19–C20	1.387(3)
C15–C16	1.467(3)	C21–C25	1.390(3)
C16–C20	1.381(3)	C22–C23	1.387(3)
C17–C18	1.391(3)	C23–C24	1.384(3)
C18–C19	1.382(3)	C24–C25	1.390(3)

In this structure each transition metal atom Co is linked by six nitrogen atoms with two thiadiazole ligands (L) in the equatorial plan and with two thiocyanate coligand ions SCN^- in apical direction, to form a distorted octahedral environment CoN_6 , with Co–N bond lengths in the range of 2.065(2)-2.161(2) Å and 2.056(2)-2.153(2) Å for Co1 and Co2 atoms, respectively, as indicated in Fig. 1. The Co–N bond lengths involving the nitrogen atoms of the SCN^- thiocyanate ions in the axial direction of the CoN_6 polyhedra, are much shorter (2.056(2)-2.065(2) Å) than those containing the nitrogen of the thiadiazole ligand (L) in the basal plane [2.134(2)-2.161(2) Å], Table 3.

Therefore, the CoN_6 octahedra are slightly axially compressed. This structural feature is typical for related compounds [17,26,40-42], and isostructural to iron complex $\text{FeL}_2(\text{NCS})_2$ described by Klingele *et al.* [43]. The iso-thiocyanate coligands bound through the nitrogen atoms and are nearly linear with $\text{N5-C13-S2} = 177.8(2)$ and $\text{N10-C26-S4} = 179.6(2)^\circ$ for Co(1) $\text{L}_2(\text{NCS})_2$ "Co(1) molecule" and Co(2) $\text{L}_2(\text{NCS})_2$ "Co(2) molecule", respectively; while the Co-NCS bond is fairly bent for Co(1) molecule with $\text{Co1-N5-C13} = 167.8(2)^\circ$, whereas is almost linear for Co(2) molecule, with an angle Co2-N10-C26 of $176.8(2)^\circ$. Similar structural properties of N-bound of NCS groups have been previously observed in the isostructural complex $\text{FeL}_2(\text{NCS})_2$ [43].

In this crystal structure each independent centrosymmetric cationic entity $[\text{CoL}_2]^{2+}$ is connected apically to two axial thiocyanate anions SCN^- to build $\text{CoL}_2(\text{SCN})_2$ complex, as indicated in the Fig. 1, where the both 2,5-bis(pyridin-2-yl)-1,3,4-thiadiazole ligands (L) adopt a *trans* configuration. The same configuration was previously observed in other cobalt complexes with the thiocyanate ion as coligand [17,26,40-42]. Indeed, the 2,5-bis(pyridine-3-yl)-1,3,4-oxadiazole ligand (L^3) adopts a *trans* conformation in $[\text{Co}(\text{L}^3)_2(\text{NCS})_2]_n$ complex and bridges two Co^{2+} centers to give a bi-dimensional layer, featuring $[\text{Co}_4(\text{L}^3)_4]$ macrocycles as subunits [40]. In the case of $[\text{Co}(\text{bpox})_2(\text{SCN})_2]\text{H}_2\text{O}$ complex, the 2,5-bis(pyridin-2-yl)-1,3,4-oxadiazole ligand *bpox* adopts a *trans* conformation, and forms hydrogen bonds with the water molecule localized in the intermolecular space [41]. The *trans* behaviour was also found in the case of Co(II) coordination complex with the same investigated ligand (L) without thiocyanate ion as coligand [17,26,42].

Thus, the crystallographically independent unit of the title compound is comprised of two different $\text{CoL}_2(\text{NCS})_2$ molecules, linked together by different weak interactions, like π - π stacking interactions as well as the various intermolecular hydrogen interactions to form a three-dimensional structure, Tables 4-5 and Fig. 2 (for the clarity of the Fig. 2, the latter is presented in the *ac* plan). Thus, the crystal cohesion is ensured by Co-N, C-H \cdots N, C-H \cdots π , C-H \cdots S interactions and π - π stacking interactions between pyridyl rings of neighbouring molecules.

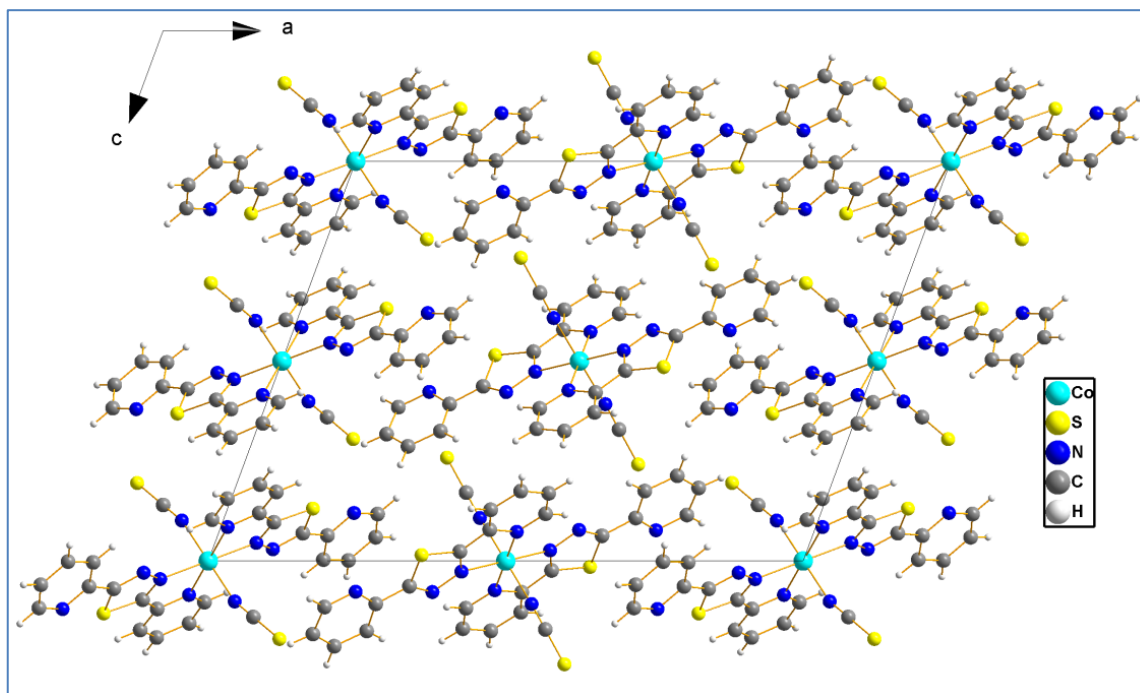


Fig. 2. Three-dimensional crystal structure view along *b* axis of $\text{CoL}_2(\text{NCS})_2$ complex.

Table 4

C–H \cdots A hydrogen-bond geometry of $\text{CoL}_2(\text{NCS})_2$ (A = N, C and S).

D–H \cdots A	D–H (Å)	H \cdots A (Å)	D \cdots A (Å)	D–H \cdots A (°)
C23–H23 \cdots N4	0.95(1)	2.722(2)	3.340(3)	123.4(1)
C13–H2 \cdots C2	0.95(1)	2.750(2)	3.619(3)	152.5(1)
C13–H4 \cdots C4	0.95(1)	2.776(2)	3.486(3)	132.2(1)
C13–H22 \cdots C22	0.95(1)	2.771(2)	3.579(3)	143.4(1)
C26–H12 \cdots C12	0.95(1)	2.860(2)	3.630(4)	138.8(1)
C26–H18 \cdots C18	0.95(1)	2.796(2)	3.670(4)	153.4(1)
C26–H20 \cdots C20	0.95(1)	2.771(2)	3.262(3)	131.5(1)
C4–H4 \cdots S2	0.95(2)	2.762(2)	3.684(3)	163.8(1)
C9–H9 \cdots S2	0.95(2)	2.872(1)	3.676(3)	143.1(1)
C24–H24 \cdots S2	0.95(2)	3.103(1)	3.567(3)	111.8(1)
C12–H12 \cdots S4	0.95(3)	2.926(1)	3.756(3)	113.1(1)
C18–H18 \cdots S4	0.95(3)	2.917(1)	3.725(3)	143.7(1)
C25–H25 \cdots S4	0.95(2)	3.043(1)	3.771(3)	134.4(1)

As indicated in the Fig. 3 and Table 4, the stabilization of the structure is supported by C–H \cdots N hydrogen bond interactions (C23–H23 \cdots N4 = 2.722(2) Å) between pyridyl rings with alternate sequences of $\cdots\text{Co}(1)\text{L}_2(\text{NCS})_2\cdots\text{Co}(2)\text{L}_2(\text{NCS})_2\cdots\text{Co}(1)\text{L}_2(\text{NCS})_2\cdots\text{Co}(2)\text{L}_2(\text{NCS})_2\cdots$, to form an infinite chain $[(\text{CoL}_2(\text{NCS})_2)_2]_\infty$.

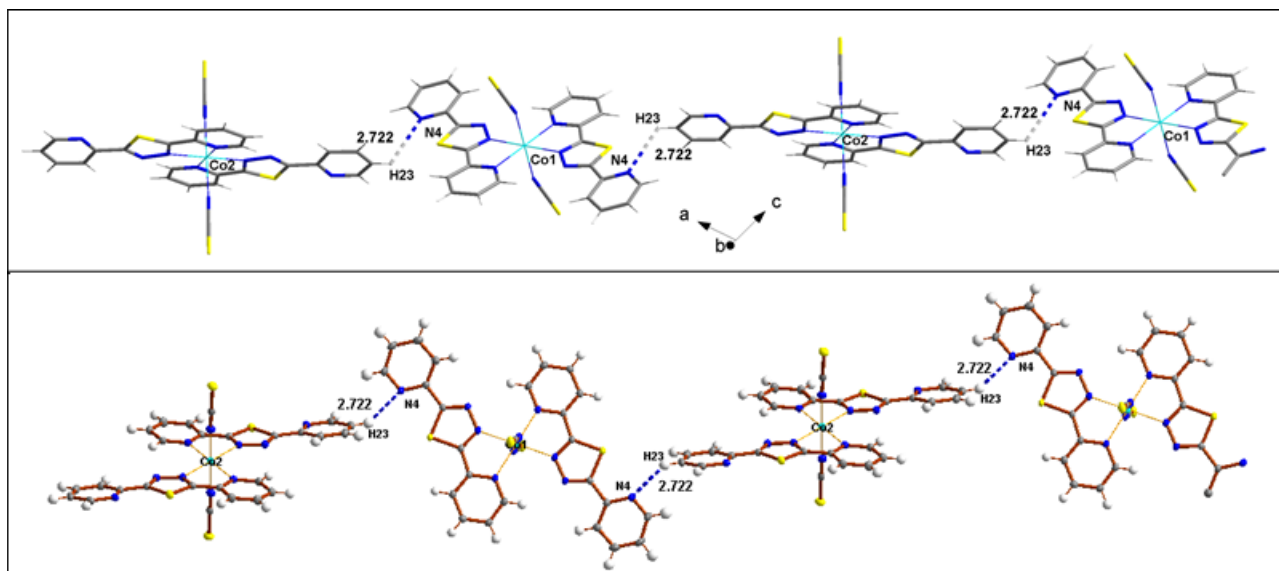


Fig. 3. Formation of infinite chain involving C23–H23...N4 hydrogen bonds in crystal structures of $\text{CoL}_2(\text{NCS})_2$.

The crystal structure is further stabilized by sulfur hydrogen C–H...S interactions as indicated for both molecules $\text{Co(1)L}_2(\text{NCS})_2$ and $\text{Co(2)L}_2(\text{NCS})_2$, and presented separately in the Fig. 4. For both $\text{CoL}_2(\text{NCS})_2$ molecules, each thiocyanate coligand shares three sulfur-hydrogen C–H...S bonds with pyridyl rings of other neighbouring molecules, with distances range from 2.762(2) to 3.103(1) Å in $\text{Co(1)L}_2(\text{NCS})_2$, and from 2.917(1) to 3.043(1) Å in $\text{Co(2)L}_2(\text{NCS})_2$, to form three dimensional network as indicated in Fig. 5.

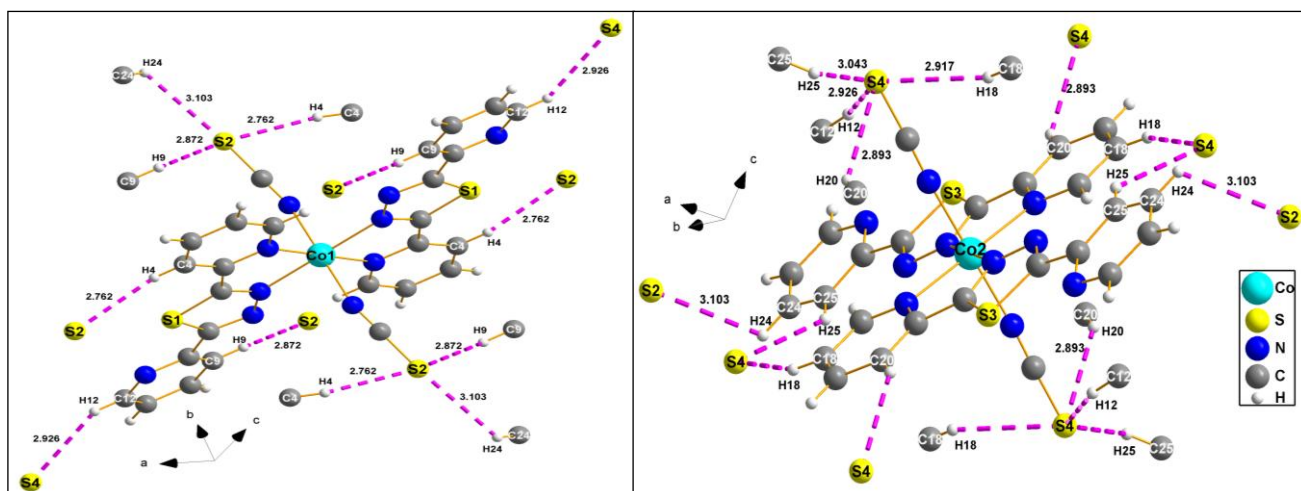


Fig. 4. Sulfur-hydrogen interactions in crystal structure of $\text{CoL}_2(\text{NCS})_2$.

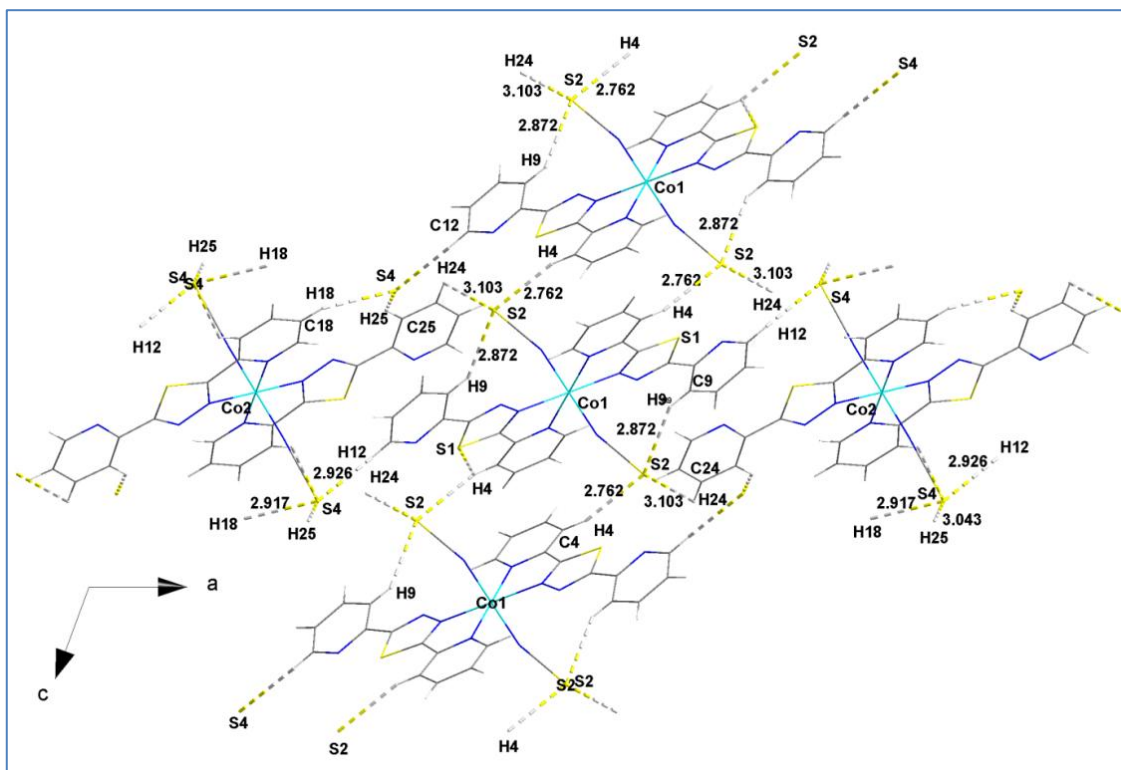


Fig. 5. Partial packing diagram of the complex showing the network of sulfur-hydrogen bonds linking of $\text{CoL}_2(\text{NCS})_2$ into layers parallel to the ac plane.

As presented in the Fig. 6 and Table 4, intermolecular $\text{C-H}\cdots\text{C}$ interactions are also formed between thiocyanate carbon atoms of each $\text{CoL}_2(\text{CNS})_2$ molecule and the pyridyl hydrogen atoms of 2,5-bis(pyridin-2-yl)-1,3,4-thiadiazole ligands, with distances in the range of 2.750–2.860 Å and 3.262–3.670 Å for $\text{H}\cdots\text{C}$ and $\text{C-H}\cdots\text{C}$, respectively.

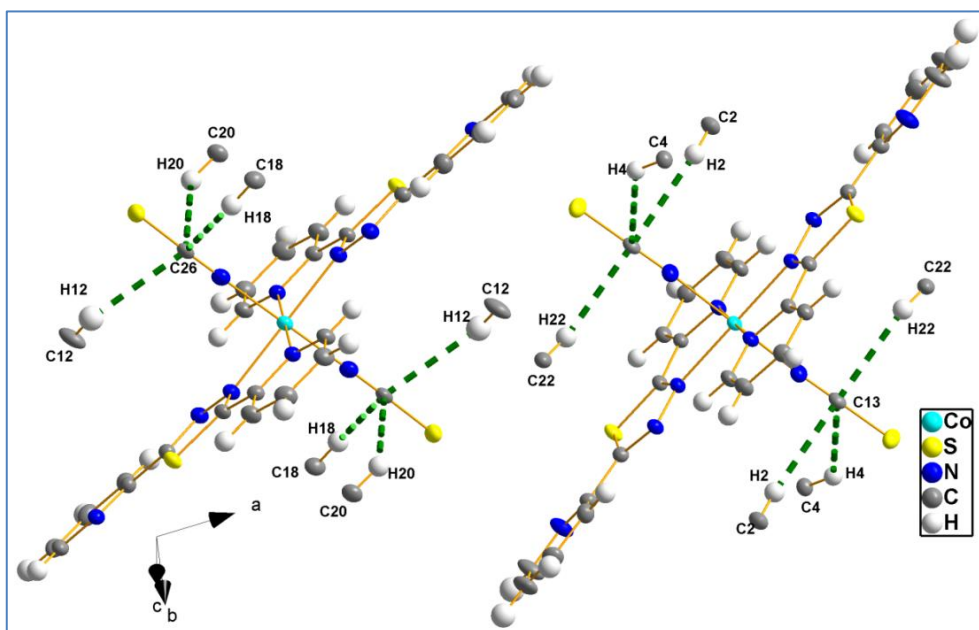


Fig. 6. Carbon Hydrogen $\text{C-H}\cdots\text{C}$ interactions in crystal structure of $\text{CoL}_2(\text{NCS})_2$.

In addition, three different intermolecular C–H \cdots π interactions are also observed between the centroids of pyridyl rings and aromatic H atoms H4 and H9 with distances of 3.370(2), 3.440(2) and 3.736(2) Å, as indicated in Table 5. These interactions also contribute to the cohesion of the structure as shown in Fig.7. They are often observed between arenes, alkenes or alkynes in hydrocarbons and play an important role in chemistry and biology [44].

Table 5

C–H \cdots π Hydrogen-bond geometry for CoL₂(NCS)₂.

C–H \cdots π	H \cdots π (Å)	C–H \cdots π (°)
C4–H4 \cdots π	3.370(2)	88.5(3)
C9–H9 \cdots π	3.440(2)	102.0(3)
C9–H9 \cdots π	3.736(2)	92.4(3)

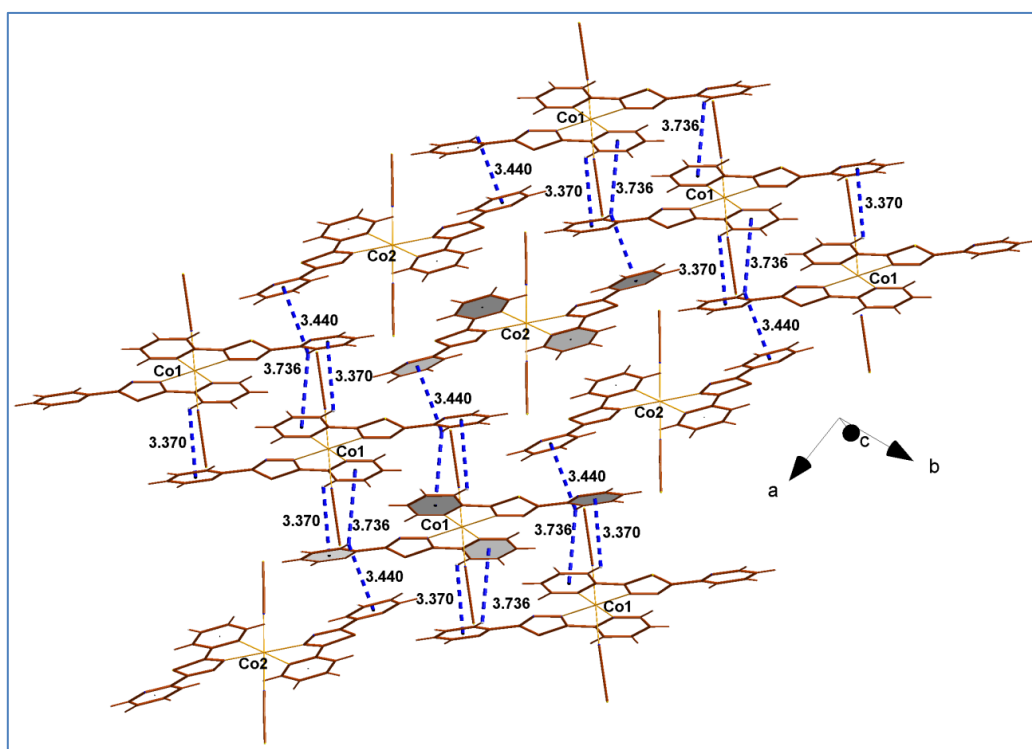


Fig. 7. C–H \cdots π stacking interactions in crystal structures of CoL₂(NCS)₂.

There are also three different π – π stacking interactions existing in crystal structure of CoL₂(NCS)₂ complex, observed between the pyridyl ring centroids of neighbouring molecules with distances range from 4.036 to 4.480 Å, as indicated in Fig. 8. Indeed, these stacking interactions

connect the molecules together and participated to the cohesion of the structure to form a 3D supramolecular structure. These interactions are often observed in the molecules containing aromatic rings and generally depend upon charge distribution and also the shape of molecule; and require geometrical requisites [45-47]. It should be also noted that these interactions are of utmost importance in drug chemistry, as most drugs are aromatic.

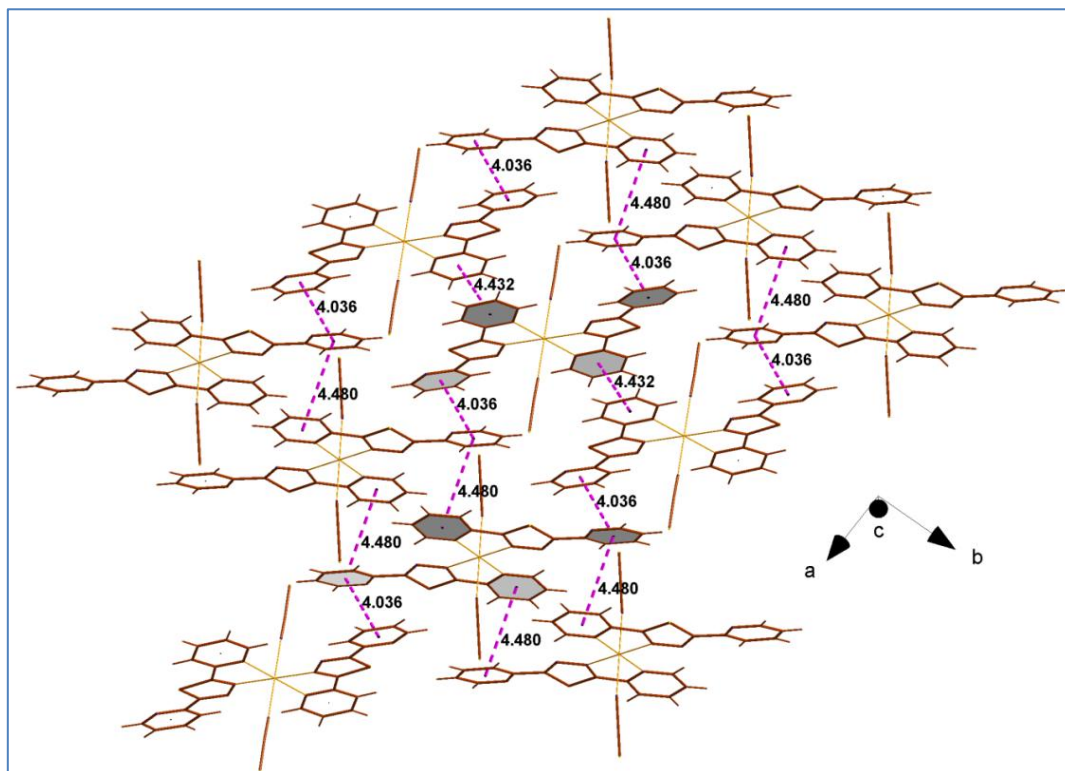


Fig. 8. π - π stacking interactions in crystal structure of $\text{CoL}_2(\text{NCS})_2$.

The purity of prepared powder of $\text{CoL}_2(\text{NCS})_2$ was also verified by powder X-ray diffraction (PXRD). The diffractogram profile refinement, in monoclinic symmetry with $P 2_1/c$ space group, was carried out according the Le Bail method [48] using the pattern matching option of Fullprof program [35], where only the profile parameters (cell dimensions, symmetry, peak shapes, and zero-point correction) have been refined. Pseudo-Voigt function with an asymmetry correction at low angles was used to describe the peak shape. The final observed, calculated, and difference PXRD patterns resulting from the profile-matching procedure are plotted in Fig. 9. Refined cell parameters with their profile reliability factors (R_p and R_{wp}) are also listed in Table 6.

The obtained structure refinement parameters showed that PXRD and crystal diffraction findings are in good agreement for $\text{CoL}_2(\text{NCS})_2$.

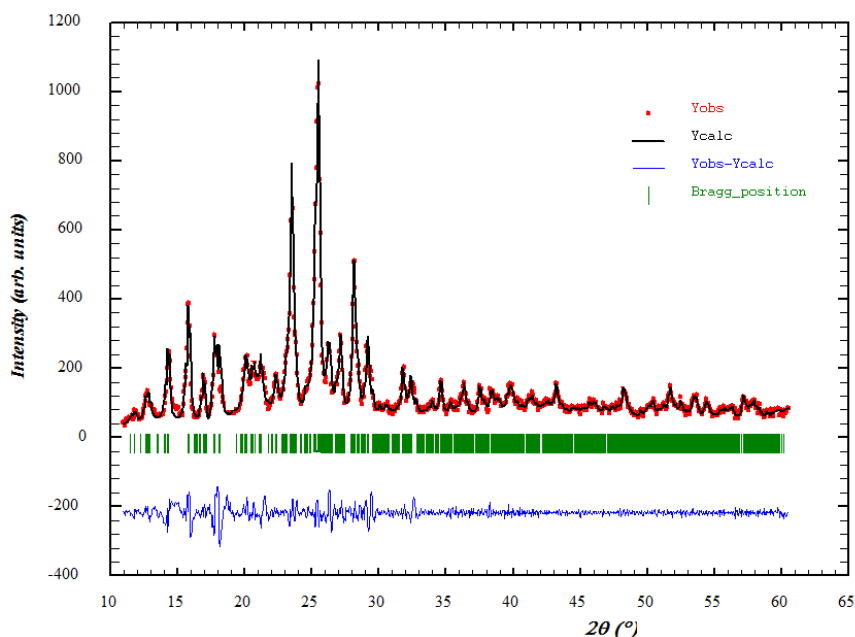


Fig. 9. Profile-matching result of $\text{CoL}_2(\text{NCS})_2$ complex using powder X-ray diffraction. The observed, calculated, and difference patterns are in red, black and blue, respectively. The small marks in green correspond to the Bragg peaks positions.

Table 6

Lattice parameters and reliability factors of $\text{CoL}_2(\text{NCS})_2$.

Complex	a (Å)	b (Å)	c (Å)	β (°)	R_p (%)	R_{wp} (%)
$\text{CoL}_2(\text{NCS})_2$	22.866 (4)	7.920 (1)	16.395 (4)	110.17 (1)	2.36	3.48

3.2. Hirshfeld surface analysis

The Hirshfeld surface was calculated for the individual $\text{Co}(1)\text{L}_2(\text{NCS})_2$ and $\text{Co}(2)\text{L}_2(\text{NCS})_2$ molecules in the title complex (Fig. 1), and for overall ($\text{CoL}_2(\text{NCS})_2$). In order to compare with an isostructural complex, the Hirshfeld surface was also performed for overall $\text{FeL}_2(\text{NCS})_2$ [43]. The three dimensional molecular Hirshfeld surfaces were generated using a high standard surface resolution for $\text{Co}(1)\text{L}_2(\text{NCS})_2$ "Co(1) molecule" and $\text{Co}(2)\text{L}_2(\text{NCS})_2$ "Co(2) molecule" for d_{norm} are

shown in Fig. 10. The red spots on the Hirshfeld surface mapped with d_{norm} correspond to the C–H···S and C–H···C interactions (Fig. 11a).

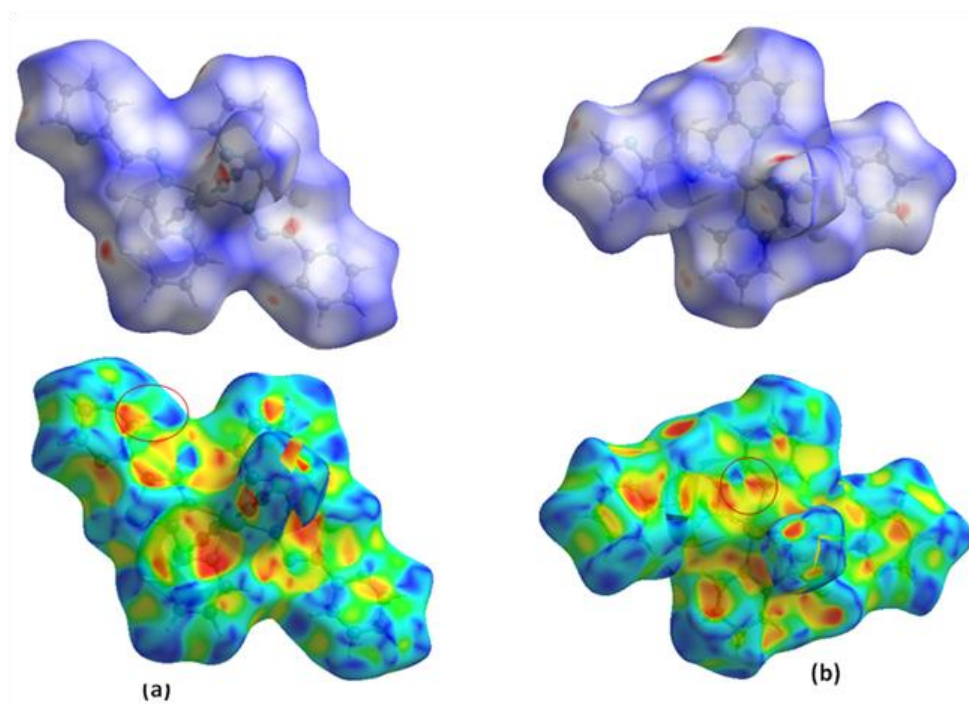


Fig. 10. Views of the Hirshfeld surfaces mapped over d_{norm} and shape-index for components of $\text{CoL}_2(\text{NCS})_2$: (a) Co(1) molecule and (b) Co(2) molecule.

The corresponding fingerprint plots for Co(1) and Co(2) molecules in $\text{CoL}_2(\text{NCS})_2$ and for overall $\text{CoL}_2(\text{NCS})_2$ as shown with characteristic pseudo-symmetric wings in the d_e and d_i diagonal axes and those delineated into C···H/H···C, S···H/H···S, N···H/H···N, H···H and C···C contacts are illustrated in Fig. 12. The percentage contributions from different interatomic contacts to their respective Hirshfeld surfaces are quantitatively summarized in Table 7. For both molecules, the contributions from C···H/H···C, S···H/H···S, N···H/H···N and H···H contacts are the largest (29.9%, 26.1%, 15.3%, 12.5% and 24.3%, 24.8%, 14.3%, 18.2% for Co(1) and Co(2) molecules respectively). The contact analysis for the investigated complex suggests that the C···H/H···C contacts (Fig. 12b) are the driving force in molecular arrangement and crystal packing formation, the largest contribution with 27.4% of the surface is from C···H contacts in C–H··· π interactions between the centroids of pyridyl rings and aromatic H-atoms H4 and H9 (Table 5), in the crystal (Fig. 11b). In the fingerprint plot delineated into S···H/H···S contacts in Fig. 12c, the pair of spikes

at $d_e + d_i \approx 2.6 \text{ \AA}$ and 2.7 \AA for the Co(1) and Co(2) molecules respectively, represent the presence of the C–H \cdots S hydrogen bonds between them. The H \cdots H ($d_e + d_i \approx 2.5 \text{ \AA}$) and H \cdots N/N \cdots H ($d_e + d_i \approx 2.6 \text{ \AA}$) contacts (Figs. 12d and 12e) makes similar contributions to the total Hirshfeld surface of 15.6 and 15.0%, respectively. H \cdots H contacts represent van der waals interactions and H \cdots N/N \cdots H correspond to hydrogen bonds.

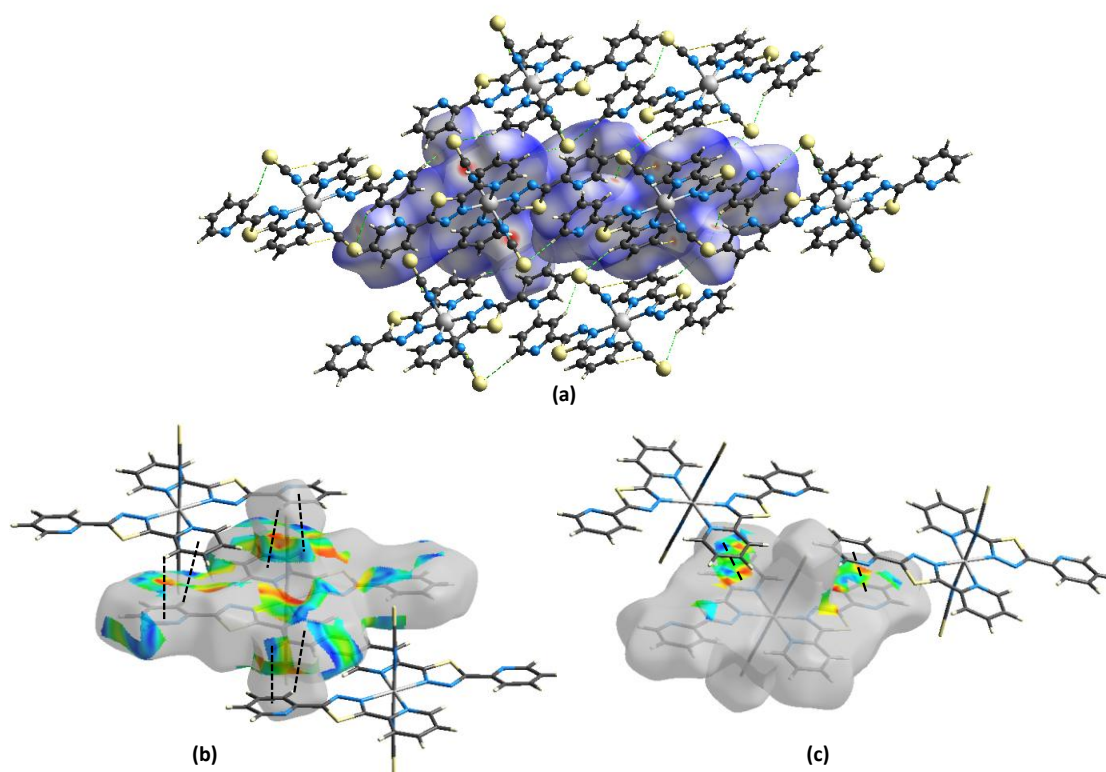


Fig. 11. Hirshfeld surfaces mapped over (a) d_{norm} to visualize the intermolecular C–H \cdots S and C–H \cdots C and shape-indexed property for Co(1) and Co(2) molecules highlighting intermolecular (b) C–H \cdots π and (c) π - π interactions through black dashed lines.

The molecules are related to one another by π - π stacking interactions with pyridine ring by the Co(1) and Co(2) molecules (Figs. 8 and 11c), as can be inferred from inspection of the adjacent red and blue triangles (highlighted by red circles) on the shape-index surface (Fig. 10). The C \cdots C contacts have an arrow-shaped distribution of points with the tip at $d_e \approx d_i \approx 1.6 \text{ \AA}$ (Fig. 12f). When the two molecules in the asymmetric unit of $\text{CoL}_2(\text{NCS})_2$ are compared with each other (Table 7), there is little difference between them. The small contributions from other remaining interatomic contacts have negligible effect on the packing. A comparison of the molecular surfaces of Hirshfeld in two complex $\text{CoL}_2(\text{NCS})_2$ and $\text{FeL}_2(\text{NCS})_2$ [43] clearly shows that the Hirshfeld surface have

similar shapes and fingerprint plots (Fig. 12), reflecting the same packaging and intermolecular patterns solid state arrangements.

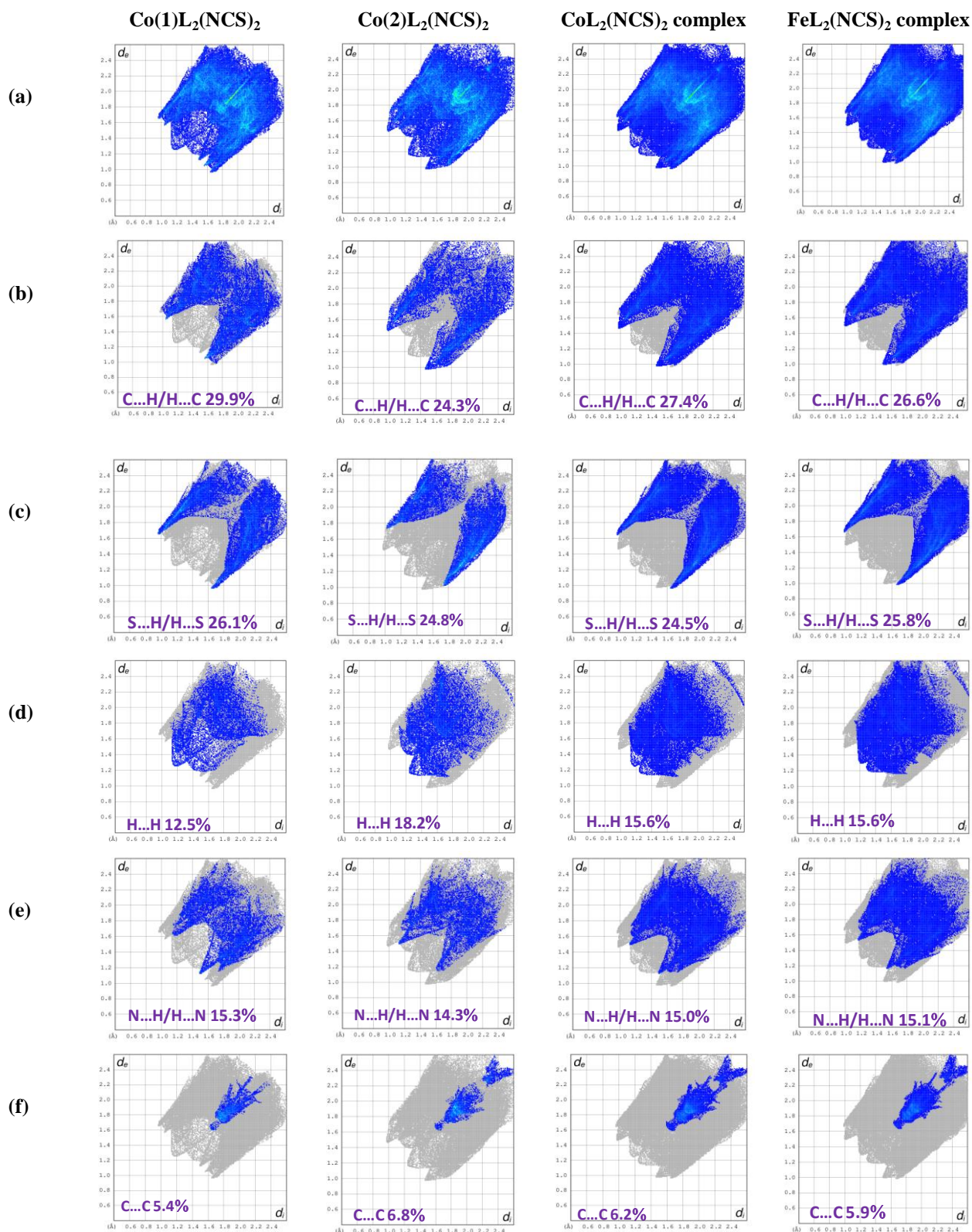


Fig. 12. (a) The full two-dimensional fingerprint plots for Co(1)L₂(NCS)₂ and Co(2)L₂(NCS)₂ molecules, overall of CoL₂(NCS)₂ and FeL₂(NCS)₂ complexes and (b)–(f) those delineated into C...H/H...C, S...H/H...S, N...H/H...N, H...H and C...C contacts in Co(1)L₂(NCS)₂ and Co(2)L₂(NCS)₂ molecules and in CoL₂(NCS)₂ and FeL₂(NCS)₂ complexes.

Table 7

Percentage contributions of interatomic contacts to the Hirshfeld surface for the $\text{Co(1)L}_2(\text{NCS})_2$ and $\text{Co(1)L}_2(\text{NCS})_2$ molecules and for overall $\text{CoL}_2(\text{NCS})_2$ complex.

Contact	Percentage contribution			
	$\text{Co(1)L}_2(\text{NCS})_2$	$\text{Co(2)L}_2(\text{NCS})_2$	$\text{CoL}_2(\text{NCS})_2$ complex	$\text{FeL}_2(\text{NCS})_2$ complex [43]
C...H/H...C	29.9	24.3	27.4	26.6
S...H/H...S	26.1	24.8	24.5	25.8
H...H	12.5	18.2	15.6	15.6
H...N/N...H	15.3	14.3	15.0	15.1
C...C	5.4	6.8	6.2	5.9
C...N/N...C	4.1	4.0	4.1	4.0
S...C/C...S	2.6	3.8	3.2	3.1
S...S	2.6	1.0	1.8	1.8
N...S/S...N	1.2	2.6	1.9	2.0
N...N	0.2	0.2	0.2	0.2

3.3. Spectroscopy studies

3.3.1. Ultraviolet-visible spectroscopy

The electronic spectra of the ligand (L) and its complex ($\text{CoL}_2(\text{NCS})_2$), are shown in Fig. 13. The absorption maxima (λ_{max}) are also shown in Table 8. If the cobalt(II) d^7 ion is in an octahedral environment, it has three transitions $d-d$ in UV-Visible spectroscopy: $\lambda_1: {}^4T_{1g}(F) \rightarrow {}^4T_{1g}(P)$, $\lambda_2: {}^4T_{1g}(F) \rightarrow {}^4A_{2g}(F)$ and $\lambda_3: {}^4T_{1g}(F) \rightarrow {}^4T_{2g}(F)$ [49,50]. The complex $\text{CoL}_2(\text{NCS})_2$ in DMSO, its electron spectrum in the visible range, effectively displays three low-intensity bands at 431(λ_1), 642(λ_2) and 796 nm (λ_3) successively attributable to the transitions mentioned above. This seems to indicate that the metal is probably hexa-coordinated. In the UV domain two more intense bands at 272 and 317 nm are assignable to the intra-ligand transitions $\pi \rightarrow \pi^*$ and $n \rightarrow \pi^*$ of L linked to the metal. These transitions should be compared with those of the free ligand L, in the same solvent, who appear at 245 and 305 nm successively [24].

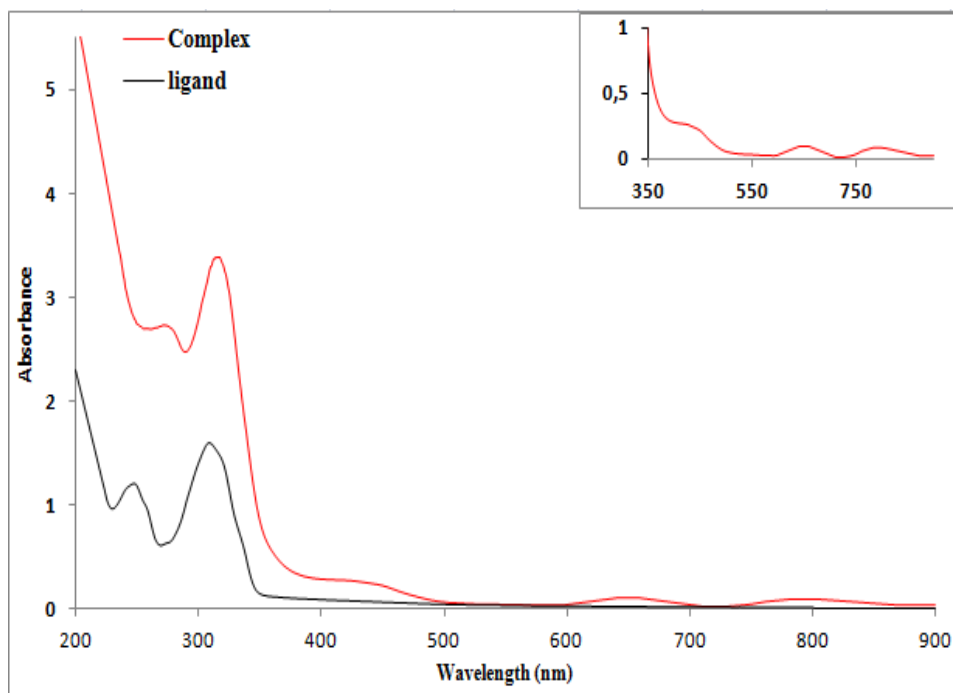


Fig. 13. Electronic spectra of the ligand L and the title complex $\text{CoL}_2(\text{NCS})_2$ in DMSO (10^{-4} M).

Table 8

Assignments of the main UV bands of the ligand (L) and of the title complex $\text{CoL}_2(\text{NCS})_2$ in DMSO (10^{-4} M).

Compound	λ_{max} (nm) (ϵ_{max} , $\text{M}^{-1} \text{cm}^{-1}$)				
	$\pi \rightarrow \pi^*$	$n \rightarrow \pi^*$	<i>d-d</i>		
Ligand	245 (11810)	305 (15700)	—		
$\text{Co(L)}_2(\text{SCN})_2$	272 (27300)	317 (33720)	431 (2620)	642 (180)	796 (860)
			${}^4\text{T}_{1g}(\text{F}) \rightarrow {}^4\text{T}_{1g}(\text{P})$	${}^4\text{T}_{1g}(\text{F}) \rightarrow {}^4\text{A}_{2g}(\text{F})$	${}^4\text{T}_{1g}(\text{F}) \rightarrow {}^4\text{T}_{2g}(\text{F})$

3.3.2. FTIR spectroscopy

The FTIR spectra of ligand and its complex are shown in Fig. 14. In infrared spectroscopy, the presence of the thiocyanate is revealed mainly by a fine and intense peak around 2100 cm^{-1} which corresponds to the $\nu_{\text{as}}(\text{CN})$ stretching of the SCN^- group. If this value is less than 2100 cm^{-1} , it is generally attributed to a terminal ligand bound by the nitrogen atom [51-53]. The IR spectrum of the complex seems to indicate, by the value of this frequency (2079 cm^{-1}) that the two thiocyanates are bound by nitrogen atom. The non-duplication of the signal suggests that the two

co-ligands are equivalent to each other in the coordination sphere of the metal. The spectrum of the studied complex also shows several absorption bands, which correspond to the different modes of vibration of the ligand L (Table 9). We note in particular those of 1636 and 642 cm^{-1} successively attributable to the C=N and C–S–C bonds.

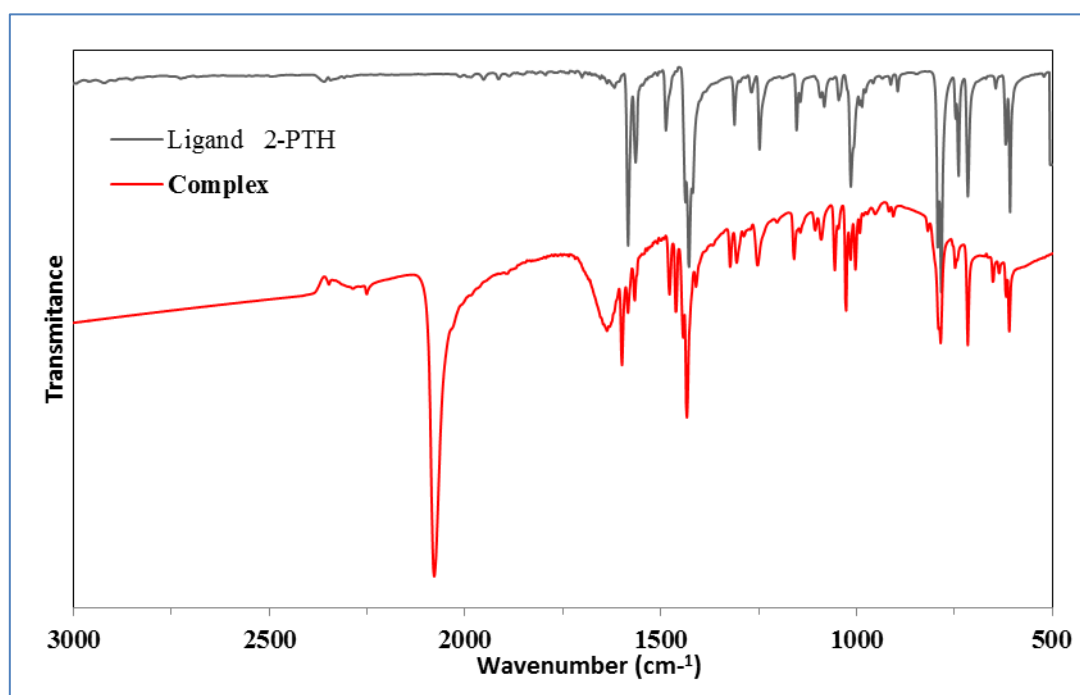


Fig.14. Infrared spectra of ligand (L) and its complex $\text{CoL}_2(\text{NCS})_2$ in the 500-3000 cm^{-1} range.

Table 9
FTIR data (cm^{-1}) of the ligand and its complex $\text{CoL}_2(\text{NCS})_2$.

Compound	$\nu(\text{C-S-C})$	$\nu(\text{C=C})$	$\nu(\text{C=N})$	$\nu(\text{NCS}^-)$
Ligand	637	1560 - 1580	—	—
Complex	642	1564 - 1600	1636	2079

3.3.3. Raman spectroscopy

Fig. 15 shows the Raman spectra of the ligand L and title complex “ $\text{CoL}_2(\text{NCS})_2$ ”. Only the main differences between the two spectra will be discussed in the following. Compared to the ligand spectrum, a new feature appears at 2072 cm^{-1} for the cobalt complex (Fig. 16). This band can be attributed to NCS^- anions [54].

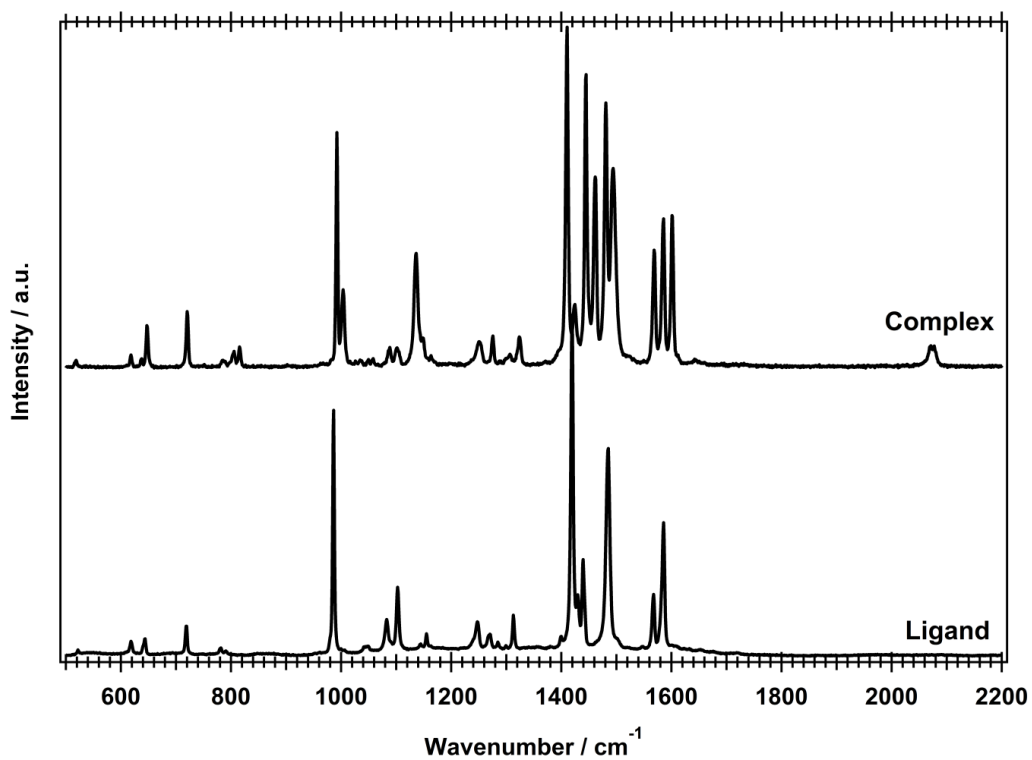


Fig. 15. Raman spectra of the ligand and its complex in the 500-2200 cm⁻¹ range.

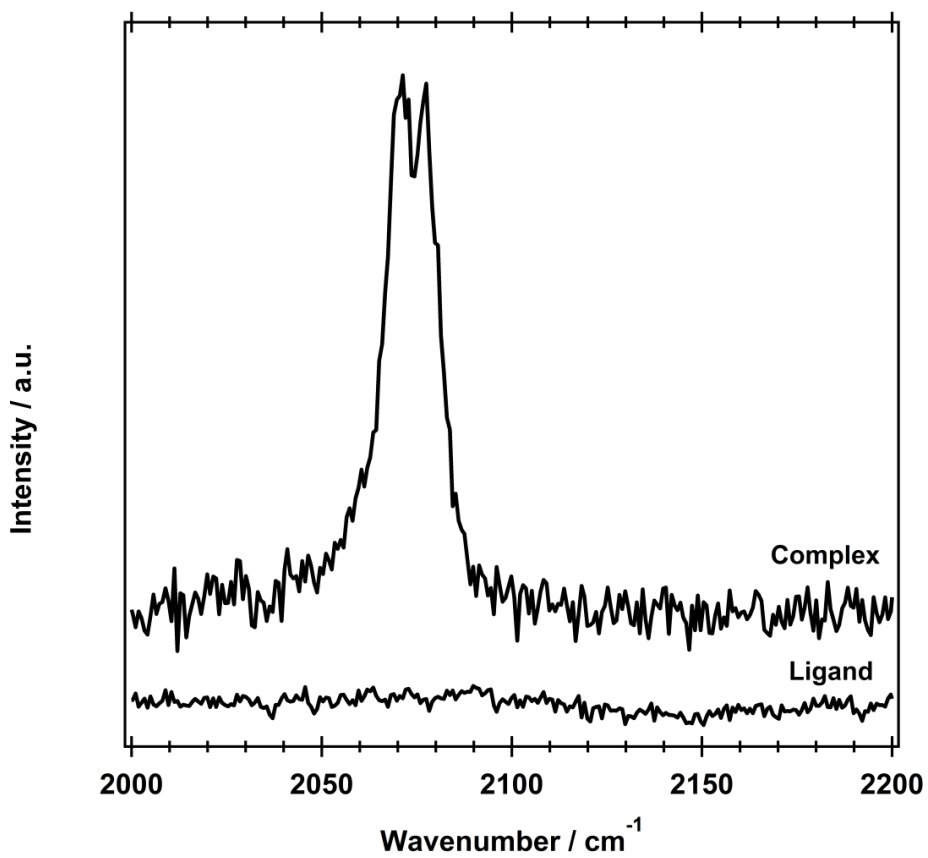


Fig. 16. Raman spectra of the ligand and its complex in the 2000-2200 cm⁻¹ range.

In the 1520-1650 cm^{-1} range, two bands at 1585 and 1567 cm^{-1} are observed for the ligand while three bands at 1601, 1585 and 1568 are obtained for the complex (Fig. 17). According to da Mota *et al.* [55], the presence of three bands for the complex instead of two for the free ligand suggests the coordination of only one pyridine group to the metal. The 1400-1500 cm^{-1} range is characteristic of C=N bonds in the thiadiazole ring as illustrated in Fig. 18 [56]. Additional bands together with slight Raman shifts are observed for the complex compared to the free ligand in this region. This can be explained by the coordination of the thiadiazole ring to the metal *via* N atom.

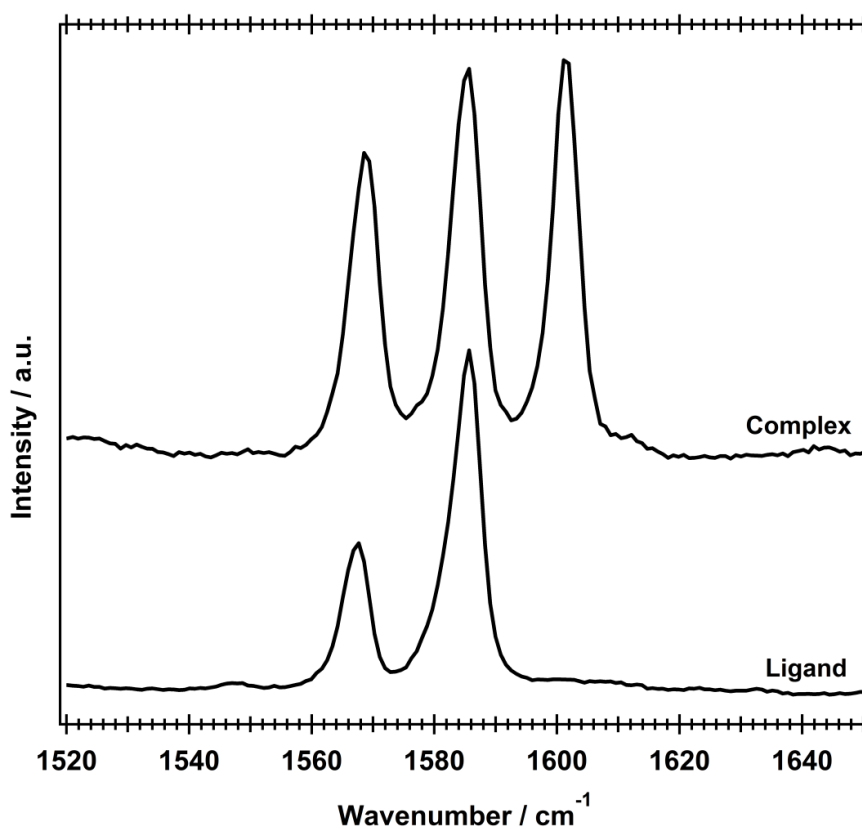


Fig. 17. Raman spectra of the ligand and its complex in the 1520-1650 cm^{-1} range.

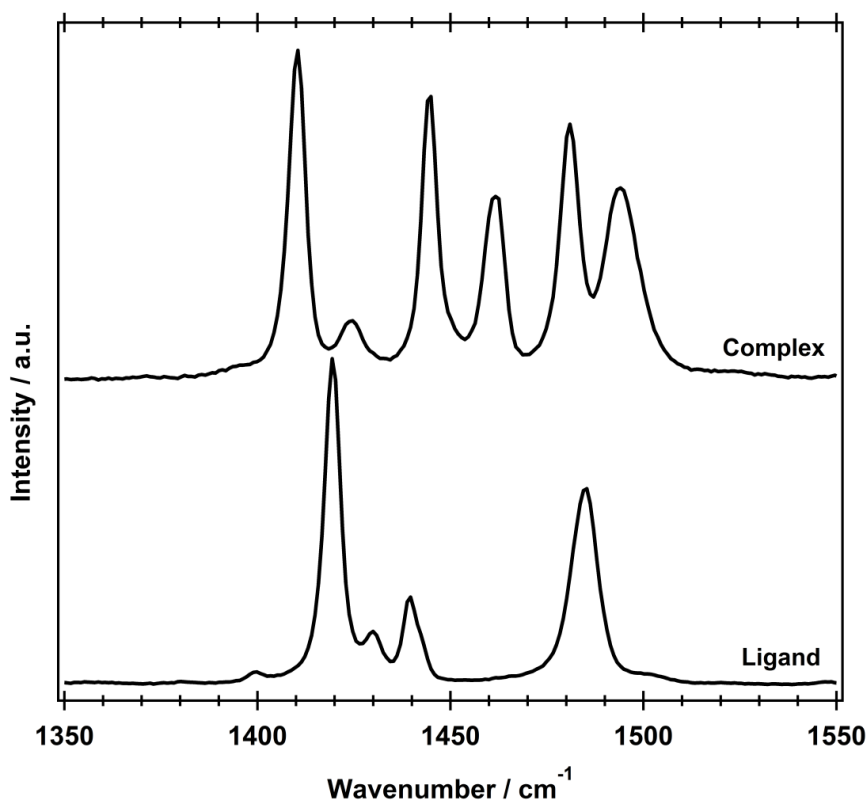
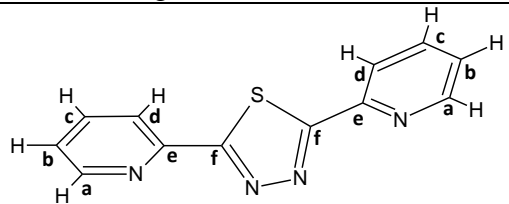


Fig. 18. Raman spectra of the ligand and its complex in the 1350-1550 cm^{-1} range.

3.3.4. ^1H and ^{13}C NMR analysis

The ^1H and ^{13}C NMR spectrum were recorded in DMSO-*d*6 for complex and compared with the corresponding spectrum of free ligand (L), as described in the literature [30]. The ^1H and ^{13}C NMR chemical shifts (δ ppm) of the 1,3,4-thiadiazole ligand (L) and its complex “ $\text{CoL}_2(\text{NCS})_2$ ” are listed in Table 10. Compared to the free ligand, some changes were observed in the proton chemical shift values of the cobalt complex. This behaviour may be due to the formation of the various intermolecular hydrogen interactions and the coordination of the thiadiazole ring to the cobalt via N atom [57]. The ^{13}C NMR signals of the ligand (L) are also slightly downfield shifted upon coordination to the cobalt metal (Table 10) [57], supporting therefore the conclusions drawn on the basis of ^1H NMR measurements. On the other hand, one more signal observed at 132.12 ppm in the case of the investigated complex was assigned to carbon atom of the isothiocyanate coordinated in $\text{CoL}_2(\text{NCS})_2$ [58].

Table 10NMR data (cm^{-1}) of the ligand and its complex $\text{CoL}_2(\text{NCS})_2$ in $\text{DMSO-}d_6$.

Position	Data free ligand	Data complex
		
^1H NMR chemical shift (δ ppm)		
H_b	7.59	7.61
H_d	8.03	8.07
H_c	8.31	8.33
H_a	8.73	8.75
^{13}C NMR chemical shift (δ ppm)		
C_b	120.56	121.05
C_d	126.22	126.73
C_c	138.02	138.52
$\text{C}_{\text{-NCS}}$	—	132.12
C_a	148.17	148.62
C_e	150.30	150.81
C_f	171.14	171.64

3.4. Thermal decomposition study

In order to ascertain its thermal stability, $\text{CoL}_2(\text{NCS})_2$ was subjected to thermogravimetric analysis (TGA) under air in the temperature range of 20–700°C and the obtained thermogram is given in Fig. 19. The TGA plot can be analyzed as having three stages of decomposition. Indeed, the cobalt complex shows a weight loss in the 200–500°C range, complying with the decomposition of the thiocyanates part and the organic ligands from the cobalt complex. The obtained experimental value is 64% which is in agreement with the theoretical value of 63.3% and complying with the possible removal of the two thiocyanate co-ligands and two thiadiazole ligands (L). The first weight loss (17.98 %) occurs between 200 and 262 °C; the second and third is an overlapping stage, with a weight loss of 46.02 % of the initial weight, take place approximately between 307 and 436°C. On the basis of the experimental mass losses, the first decomposition step can be ascribed to the loss of the two thiocyanate co-ligands (calc. 17.7%) [59]. In the higher-temperature stage, the overlapping decomposition steps can be attributed to the successive loss of two 1,3,4-thiadiazole ligands (L) to form a metallic oxide Co_3O_4 as a residual mass (calcd. 45.7%).

The formation of the cobalt oxide was confirmed by Energy Dispersive X-Ray analysis (EDX). The good thermal stability of the $\text{CoL}_2(\text{NCS})_2$ complex is supported by the thermal decomposition data showing that the investigated cobalt complex is thermally stable up to 200°C .

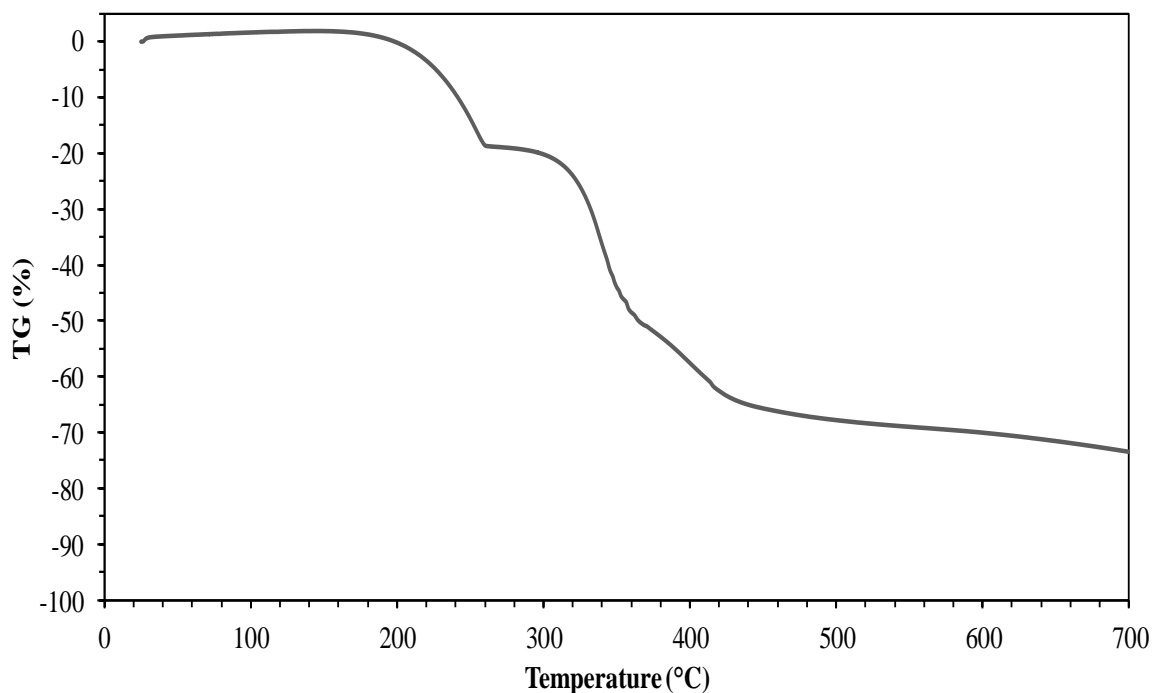


Fig. 19. TGA analysis of $\text{CoL}_2(\text{NCS})_2$ in air with a heating rate of 5 K/min.

3.5. Magnetic properties

The bivalent transition metals (Mn^{II} , Fe^{II} and Co^{II}) based coordination compounds have attracted considerable attention due to their magnetism [43,60-66]. Thus, preliminary magnetic study of our complex has been also performed under an applied magnetic field of 500 Oe in temperature range 2-300 K. Before measurement, the crystallographic phase purity of crushed crystalline samples was confirmed by Powder X-Ray Diffraction analysis. The temperature dependence of the magnetic susceptibility of $\text{CoL}_2(\text{NCS})_2$ complex in the form of χ and χ^*T is shown in Fig. 20. As observed in the structure determination section above, the crystal structure of $\text{CoL}_2(\text{NCS})_2$ complex consists of a 3D network arrangement, in which two Co^{II} ions are separated by large distances and no plausible exchange interactions are possible. The experimental χ^*T value

at room temperature is $5.99 \text{ emu K mol}^{-1}$, which is much higher than the expected spin-only value of $3.76 \text{ emu K mol}^{-1}$ for two free high-spin Co^{II} ions (with for $S = 3/2$ and $g = 2$) in an octahedral coordination environment, indicating the spin-orbit coupling. This is due to orbital contribution typical for the ${}^4\text{T}_{1g}$ ground state of octahedral high-spin Co^{II} ions [65,67-70]. In addition, as the temperature decreases, the value of χ^*T decreases down to $0.24 \text{ emu K mol}^{-1}$ at 2K, which indicates an antiferromagnetic coupling between the Co^{II} ions.

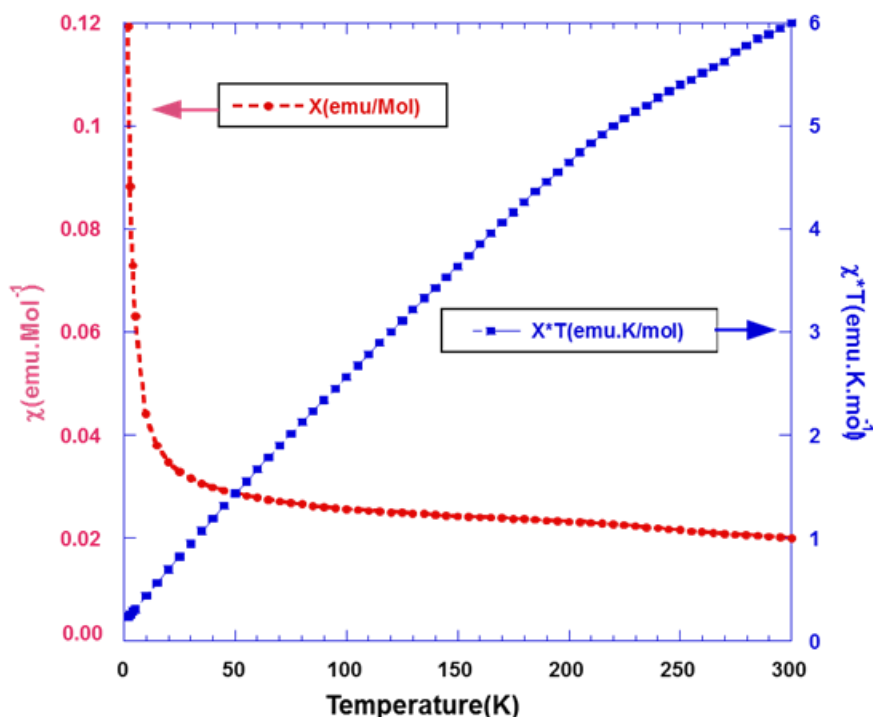


Fig. 20. Magnetic susceptibility χ^*T and χ versus temperature for $\text{CoL}_2(\text{NCS})_2$ complex.

Thus, there are two non-equivalent Co^{II} magnetic sites (Co1 and Co2) which are aligned in 3D arrangement, where the spins are constrained to be aligned either parallel or antiparallel to the easy axis, in which magnetic moments of Co1 atom are antiparallel to that of Co2 atom to give an overall antiferromagnetic interaction, with a ferrimagnetic behaviour as shown in the plot of inverse susceptibility χ^{-1} versus temperature from 2 to 300K, Fig. 21.

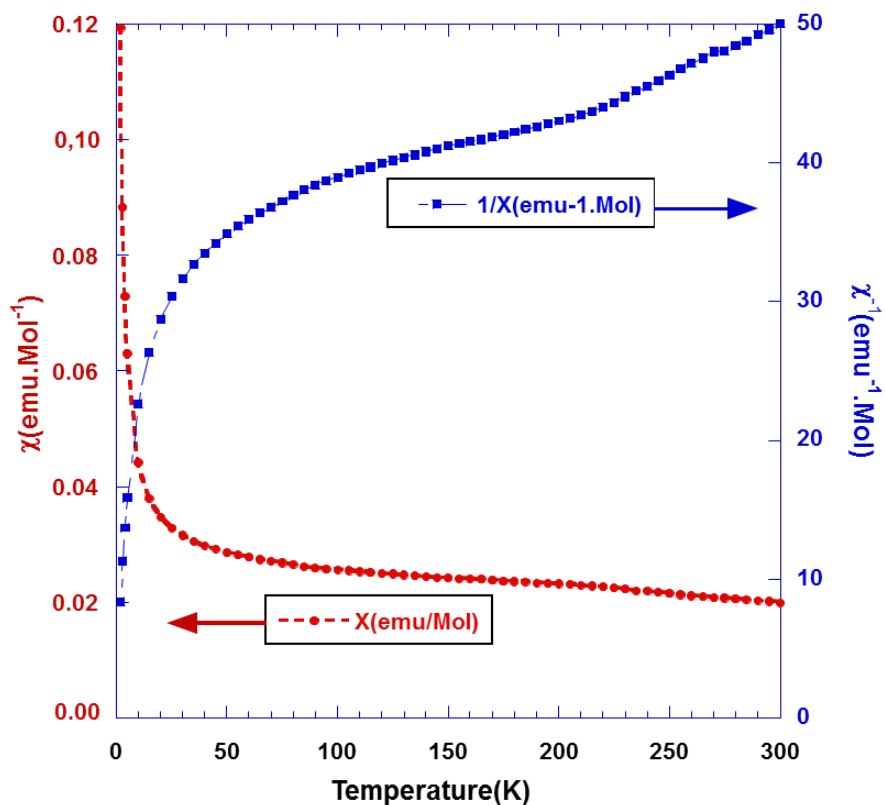


Fig. 21. Magnetic susceptibility χ and inverse χ^{-1} versus temperature from 2 to 300K for $\text{CoL}_2(\text{NCS})_2$ complex.

As shown in Fig. 22, the plot of inverse susceptibility χ^{-1} in the temperature range 2 to 50 K, reveals the important increase of susceptibility indicates a ferrimagnetic behaviour, with a para to ferrimagnetic transition at low temperature ($T_c \approx 2$ K); confirmed by hysteresis M(H) curve at 2K.

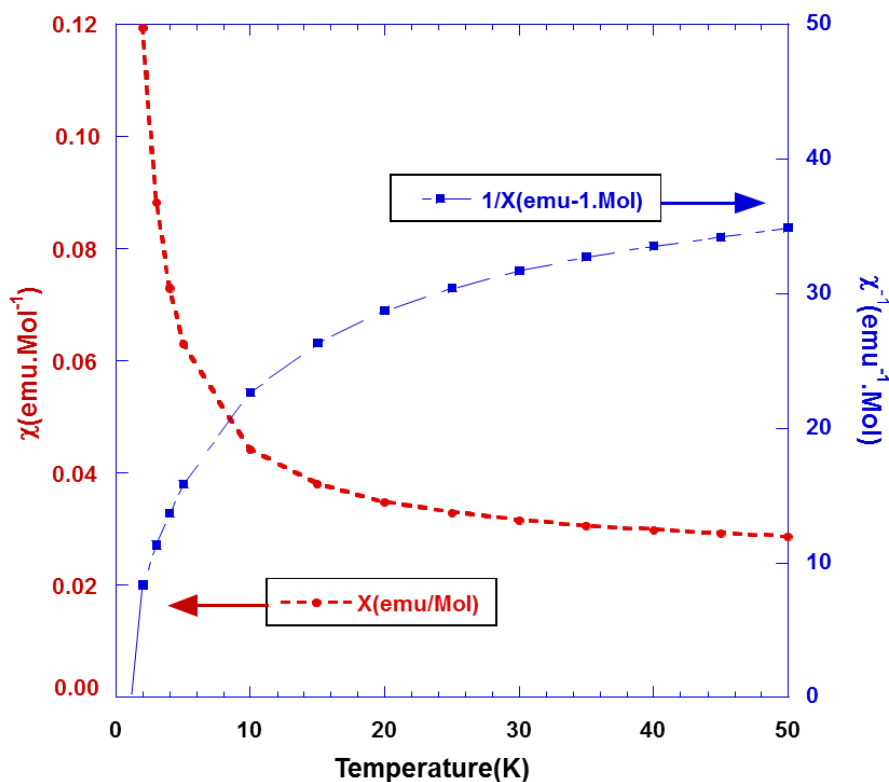


Fig. 22. Magnetic susceptibility χ and inverse χ^{-1} versus temperature from 2 to 50 K for $\text{CoL}_2(\text{NCS})_2$.

It is also interesting to compare the thermal-magnetic behaviours between our compound $\text{Co}^{\text{II}}(\text{L})_2(\text{NCS})_2$ and the iron isostructural complex $\text{Fe}^{\text{II}}(\text{L})_2(\text{NCS})_2$, prepared by reaction under protective atmosphere of argon, using $\text{Fe}(\text{NCS})_2$ in MeOH with a 2 : 1 ligand-to-metal molar ratio [43]. As shown in thermal-magnetic behaviours of both compounds in Fig. 232, two different magnetic evolutions were observed: in the case of cobalt complex $\text{Co}^{\text{II}}(\text{L})_2(\text{NCS})_2$ only a para-ferrimagnetic transition has been observed at low temperature (Figs. 22 and 23a), whereas in the case of $\text{Fe}^{\text{II}}(\text{L})_2(\text{NCS})_2$, Klingele *et al.* have highlighted two step spin crossover, corresponding to two magnetic transitions, as presented in Fig. 23b and confirmed by Mössbauer measurements [43]. These both magnetic transitions correspond exactly to a switch from a high-spin (HS at at 167 K) to a low-spin (LS at 112 K), through an intermediate magnetic phase between the two transition temperatures. It should also be noted that this ferrimagnetic behavior with a strong antiferromagnetic interaction at low temperature, has already been observed in some transition metal complexes previously described [70-73].

The occurrence of such weak ferrimagnetic ordering has been additionally characterized by the magnetic field-dependent isothermal magnetization $M(H)$ at 2.0 K, with magnetic field up to 6 T (Fig. 24a). It is noticeable that a typical hysteresis curve for the ferrimagnetic behaviour is well observed at 2.0 K, as frequently observed in ferrimagnetic molecular systems; with a negligible coercive field (H_c) and remanent magnetization (M_r). Thus, the $M(H)$ hysteresis curve shows a quick increase with increasing magnetic field, reaching a value of 4.0 emu g^{-1} at 15 T, then slowly increasing, attaining 5.7 emu g^{-1} for 6 T. As indicated in Fig. 24b, the coercivity field (H_c) is found to be equal to 7.5 Oe and, while remanent magnetization (M_r) is estimated to 0.008 emu g^{-1} .

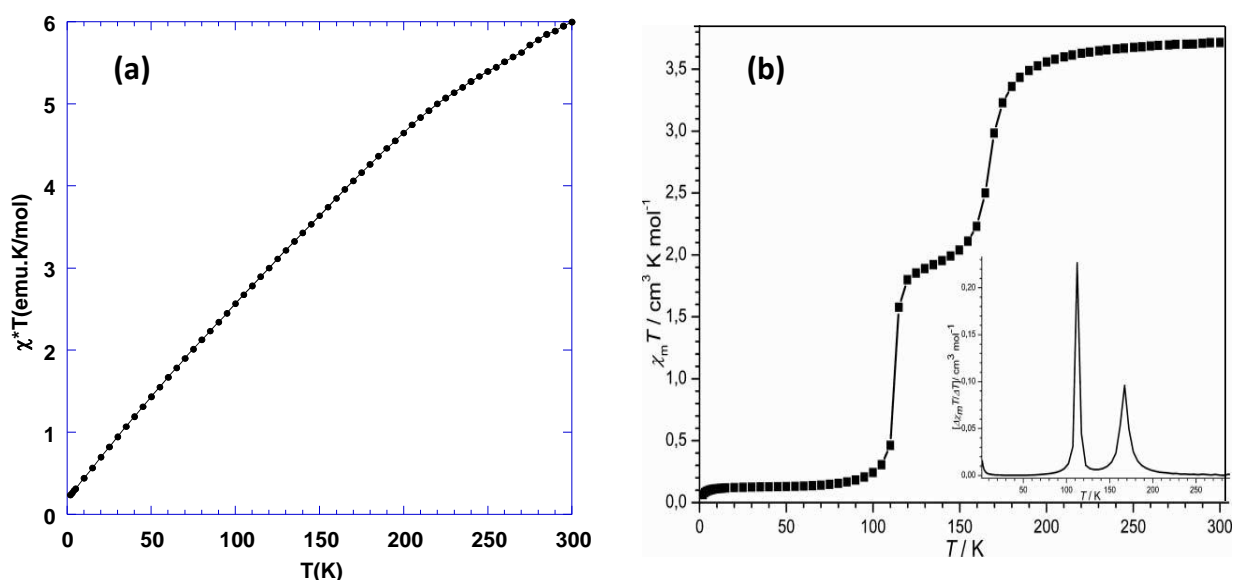


Fig. 23. χT vs. T plot for (a) $\text{Co}^{\text{II}}(\text{L})_2(\text{NCS})_2$ and (b) $\text{Fe}^{\text{II}}(\text{L})_2(\text{NCS})_2$ [41]. The inset in (b) shows the first temperature derivative of the χT .

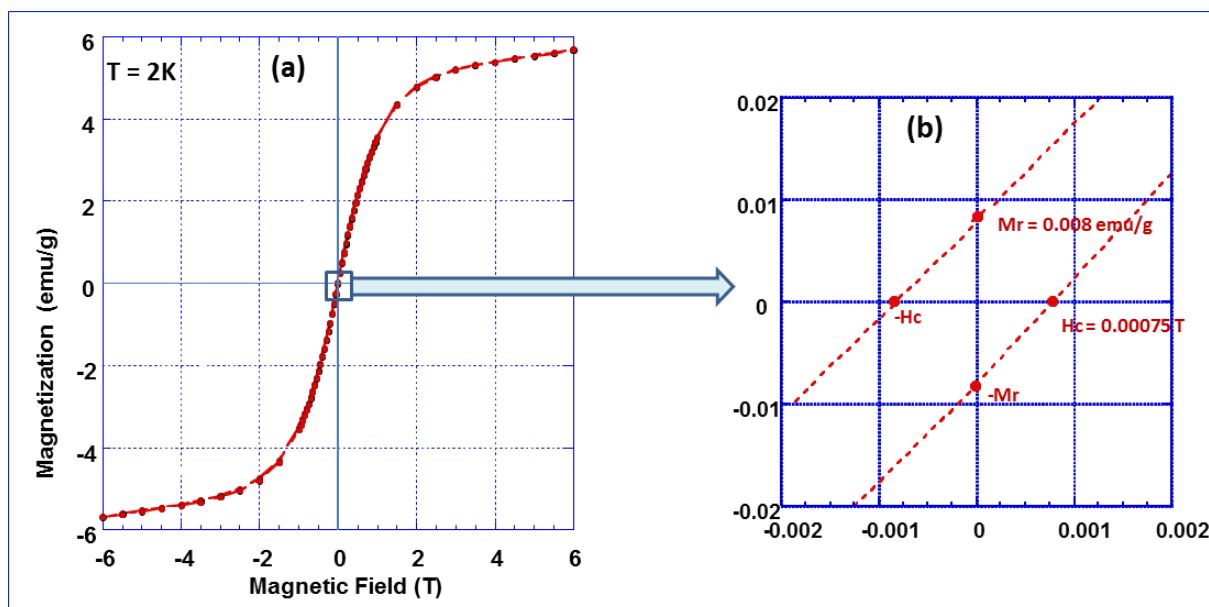


Fig. 24. Magnetic hysteresis loop for $\text{CoL}_2(\text{NCS})_2$ at 2K.

4. Conclusions

Bis(2,5-di(pyridin-2-yl)-1,3,4-thiadiazole- κ^2N,N')-bis(thiocyanato- κ^1N)cobalt(II) complex has been synthesized and its crystal structure has been characterised by single-crystal X-ray diffraction and different spectroscopic techniques (UV-Visible, FTIR, Raman, and NMR). The obtained structure presents two independent Co(II) atoms in octahedral environment, with two thiadiazole molecules acting as bidentate ligands (L) with a *trans* coordination mode and two axially coordinated thiocyanate SCN^- ions to form neutral coordination complexes $(\text{CoL}_2(\text{SCN})_2)$. The crystal structure is mainly stabilized by intermolecular hydrogen bonding, $\text{C-H}\cdots\pi$ and $\pi\cdots\pi$ stacking; in addition to the N-Co coordination bonds. Indeed, the stabilization of the structure is supported by $\text{C-H}\cdots\text{N}$ hydrogen bond interactions between pyridyl rings with alternate cobalt sequences " $\text{CoL}_2(\text{NCS})_2$ " to form an infinite chain $[(\text{CoL}_2(\text{NCS})_2)_2]_\infty$. Three-dimensional Hirshfeld surface analysis and two-dimensional fingerprint maps revealed that the $\text{C}\cdots\text{H}/\text{H}\cdots\text{C}$ and $\text{S}\cdots\text{H}/\text{H}\cdots\text{S}$ contacts represent an important contribution of the Hirshfeld surface result of hydrogen-bonding interactions in $\text{CoL}_2(\text{SCN})_2$. Thermal decomposition study reveals that the investigated complex is thermally stable up to 200 °C. Magnetic measurements showed an

antiferromagnetic exchange between the two non-equivalent cobalt(II) ions in $\text{CoL}_2(\text{SCN})_2$ complex with a ferrimagnetic behavior at low temperature.

Supplementary material

CCDC 1878437 contains the supplementary crystallographic data for $\text{Co}(\text{C}_{12}\text{H}_8\text{N}_4\text{S})_2(\text{NCS})_2$. These data can be obtained free of charge via www.ccdc.cam.ac.uk/data_request/cif, or by emailing data_request@ccdc.cam.ac.uk, or by contacting the Cambridge Crystallographic Data Centre, 12 Union Road, Cambridge CB2 1EZ, UK; fax: +44 1223 336033.

Acknowledgements

The authors are greatly thankful to the CUR CA2D of Chouaib Doukkali University for its support and UCA-PARTNER for the use of the Bruker SC diffractometer.

References

- [1] S. Li, J.-X. Chen, Q.-X. Xiang, L.-Q. Zhang, C.-H. Zhou, J.-Q. Xie, L. Yu, F.-Z. Li, *Eur. J. Med. Chem.* 84 (2014) 677–686.
- [2] U.O. Ozdemir, N. Ozbek, Z.K. Genc, A.B. Gündüzalp, *J. Mol. Struct.* 1138 (2017) 55–63.
- [3] S. Chandra, Vandana, S. Kumar, *Spectrochim. Acta A* 135 (2015) 356–363.
- [4] H.-Q. Chang, L. Jia, J. Xu, Z.-Q. Xu, R.-H. Chen, W.-N. Wu, H.-Y. Bie, T.-F. Zhu, T.-l. Ma, Y. Wang, *Inorg. Chem. Commun.* 57 (2015) 8–10.
- [5] L. Jia, J. Xu, X. Zhao, S. Shen, T. Zhou, Z. Xu, T. Zhu, R. Chen, T. Ma, J. Xie, K. Dong, J. Huang, *J. Inorg. Biochem.* 159 (2016) 107–119.
- [6] X.-Z. Zou, J.-A. Zhang, L.-J. Zhang, Y.-J. Liu, N. Li, Y. Li, S.-C. Wei, M. Pan, *Inorg. Chem. Commun.* 54 (2015) 21–24.
- [7] M.S. Muneera, J. Joseph, *J. Photochem. Photobiol.* 163 (2016) 57–68.
- [8] D.P. Singh, D.S. Raghuvanshi, K.N. Singh, V. P. Singh, *J. Mol. Catal. Chem.* 379 (2013) 21–29.
- [9] J. Mondal, A. Dutta, P.K. Pal, R. Saha, P. Maji, G.K. Patra, *Inorg. Chim. Acta* 448 (2016) 70–77.
- [10] D. Silva, M. Chioua, A. Samadi, M.C. Carreiras, M.-L. Jimeno, E. Mendes, C.D.L. Ríos, A. Romero, M. Villarroya, M.G. López, J. Marco-Contelles, *Eur. J. Med. Chem.* 46 (2011) 4676–4681.
- [11] J. Klingele, D. Kaase, M. Schmucker, L. Meier, *Eur. J. Inorg. Chem.* 28 (2013) 4931–4939.
- [12] T. Huxel, M. Skaisgirski, J. Klingele, *Polyhedron* 93 (2015) 28–36.
- [13] J.R.A. Cottam, P.J. Steel, *Inorg. Chim. Acta* 413 (2014) 160–165.
- [14] A.A. Shabana, I.S. Butler, D.F.R. Gilson, B.J. Jean-Claude, Z.S. Mouhri, M.M. Mostafa, S.I. Mostafa, *Inorg. Chim. Acta* 423 (2014) 242–255.
- [15] S.A. Elsayed, I.S. Butler, B.J. Claude, S.I. Mostafa, *Transit. Met. Chem.* 40 (2015) 179–187.
- [16] J.D.C. Almeida, I.M. Marzano, M. Pivatto, N.P. Lopes, A.M.D.C. Ferreira, F.R. Pavan, I.C. Silva, E.C. Pereira-Maia, G.V. Poelhsitz, W. Guerra, *Inorg. Chim. Acta* 446 (2016) 87–92.
- [17] F. Bentiss, M. Lagrenée, J.P. Wignacourt, E.M. Holt, *Polyhedron* 21 (2002) 403–408.
- [18] C.-Yuan. Niu, B.-L. Wu, X.-F. Zheng, X.-S. Wan, H.-Y. Zhang, Y.-Y. Niua, L.-Y. Meng, *CrystEngComm* 11 (2009) 1373–1382.
- [19] F. Bentiss, M. Lagrenée, O. Mentré, P. Conflant, H. Vezin, J.P. Wignacourt, E.M. Hol, *Inorg. Chem.* 43 (2004) 1865–1873.
- [20] D. Kaase, J. Klingele, *Acta Cryst.* E70 (2014) m252–m253.
- [21] J. Klingele, D. Kaase, M. H. Klingele, J. Lach, *Dalton Trans.* 41 (2012) 1397–1406.
- [22] X.-F. Zheng, X.-S. Wan, W. Liu, C.-Y. Niu, C.-H. Kou, *Z. Kristallogr.* 221 (2006) 543–544.
- [23] H. Zine, L.A. Rifai, M. Faize, F. Bentiss, S. Guesmi, A. Laachir, A. Smaili, K. Makroum, A. Sahibed-Dine, T. Koussa, *J. Agric. Food Chem.* 64 (2016) 2661–2267.
- [24] H. Zine, L.A. Rifai, T. Koussa, F. Bentiss, S. Guesmi, A. Laachir, K. Makroum, M. Belfaiza, M. Faize, (2017). *Pest Manag. Sci.* 73 (2016) 188–197.
- [25] A. Laachir, F. Bentiss, S. Guesmi, M. Saadi, L. El Ammari, *Acta Cryst.* E71 (2015) m24–m25.
- [26] A. Laachir, F. Bentiss, S. Guesmi, M. Saadi, L. El Ammari, *Acta Cryst.* E71 (2015) 452–454
- [27] A. Laachir, S. Guesmi, M. Saadi, L. El Ammari, O. Mentré, H. Vezin, S. Colis, F. Bentiss, *J. Mol. Struct.* 1123 (2006) 400–406.
- [28] A. Laachir, F. Bentiss, S. Guesmi, M. Saadi, L. El Ammari, *Acta Cryst.* E72 (2016) 1176–1178.
- [29] J.-G. Wang, *Z. Kristallogr. NCS* 234 (2019) 41–42.
- [30] M. Lebrini, F. Bentiss, M. Lagrenée, *J. Heterocycl. Chem.* 42 (2005) 991–995.
- [31] Bruker, APEX2. Bruker AXS Inc., Madison, Wisconsin, USA, 2012.
- [32] Bruker, SAINT. Bruker AXS Inc., Madison, Wisconsin, USA, 2012.
- [33] Bruker, SADABS. Bruker AXS Inc., Madison, Wisconsin, USA, 2012.
- [34] G.M. Sheldrick, *Acta Cryst.* C71 (2015) 3–8.
- [35] Rodriguez-Carvajal, J. FULPROF 2006: A graphic tool for powder diffraction; Version July 2006.
- [36] H.M. Rietveld, *Acta Cryst.* 22 (1967) 151–152.
- [37] M.A. Spackman, D. Jayatilaka, *CrystEngComm* 11 (2009) 19–32
- [38] J.J. McKinnon, D. Jayatilaka, M.A. Spackman, *Chem. Commun.* (2007) 3814–3816.
- [39] M.J. Turner, J.J. McKinnon, S.K. Wolff, D.J. Grimwood, P.R. Spackman, D. Jayatilaka, M.A. Spackman, *CrystalExplorer17*, The University of Western Australia, 2017.
- [40] Z. Huang, H. B. Song, M. Du, S.T. Chen, X. H. Bu, J. Ribas, *Inorg. Chem.* 43(2004) 931–944.

- [41] F. Rhoufal, A. Laachir, S. Guesmi, L. Jouffret, N. Sergent, S. Obbade, M. Akkurt, F. Bentiss, *ChemistrySelect* 4 (2019) 7773–7783.
- [42] F. Bentiss, F. Capet, M. Lagrenée, M. Saadi, L. El Ammari, *Acta Cryst. E* 67 (2011) m834–m835.
- [43] J. Klingele, D. Kaase, M.H. Klingele, J. Lach, S. Demeshko, *Dalton Trans.* 39 (2010) 1689–1691.
- [44] M. Nishio, M. Hirota, Y. Umezawa, *The CH/ π Interaction. Evidence, Nature and Consequences*; Wiley-VCH: New York, 1998.
- [45] W.B. Jennings, B.M. Farrell, J.F. Malone, *Acc. Chem. Res.* 34 (2001) 885–894.
- [46] T. Dahl, *Acta Chem. Scand.* 48 (1994) 95–106.
- [47] C.A. Hunter, *Chem. Soc. Rev.* 23 (1994) 101–109.
- [48] A. Le Bail, H. Duroy, J.L. Fourquet, Ab-initio structure determination of LiSbWO₆ by X-ray powder diffraction. *Mater. Res. Bull.* 23(3) (1988) 447–452
- [49] N. Raman, A. Kulandaisamy, A. Shunmugasundaram, K. Jeyasubramanian, *Transit. Met. Chem.* 26 (2001) 131–135.
- [50] S.C. Manna, S. Mistri, E. Zangrando, *Inorg. Chim. Acta* 413 (2014) 166–173.
- [51] R. Uhrecky, I. Ondrejovicová, D. Lacková, Z. Fáberová, J. Mrozinski, B. Kalinska, Z. Padelková, M. Koman, *Inorg. Chim. Acta* 414 (2014) 33–38.
- [52] P. Mukherjee, C. Biswas, M.G.B. Drew, A. Ghosh, *Polyhedron* 26 (2007) 3121–3128.
- [53] A. Hazari, L.K. Das, A. Bauzá, A. Frontera, A. Ghosh, *Dalton Trans.* 43 (2014) 8007–8015.
- [54] K. Nakamoto, *Infrared and raman spectra of inorganic and coordination compounds: Part B: Applications in coordination, Organometallic, and Bioinorganic Chemistry*, Sixth Edition 2008, John Wiley & Sons, Inc, p. 424.
- [55] M.M. da Mota, J. Rodgers, S.M. Nelson, *J. Chem. Soc. A* 13 (1969) 2036–2044.
- [56] T.A. Mohamed, A.E. Hassan, I.A. Shaaban, A.M. Abuelela, W.M. Zoghaib, *J. Mol. Struct.* 1130 (2017), 434–441.
- [57] A. Hannachi, A. Valkonen, M. Rzaigui, W. Smirani, *Polyhedron* 161 (2019) 222–230.
- [58] M. Daković, Z. Popović, G. Giester, and M. Rajić-Linarić, *Polyhedron* 27 (2008) 210–222.
- [59] J. Chakraborty, B. Samanta, G. Rosair, V. Gramlich, M.S. El Fallah, J. Ribas, T. Matsushita, S. Mitra, *Polyhedron* 25 (2006) 3006–3016.
- [60] C. Livage, C. Egger, M. Nogues, G. Férey, *J. Mater. Chem.* 8 (1998) 2743–2747.
- [61] J.-P. Li, Y.-Q. Ma, L.-H. Geng, Y.-H. Li, F.-Y. Yi, *CrystEngComm* 17 (2015) 6471–6475.
- [62] M. Kurmoo, H. Kumagai, S. M. Hughes, C. J. Kepert, *Inorg. Chem.* 42 (2003) 6709–6722.
- [63] J.-Y. Zou, W. Shi, H.-L. Gao, J.-Z. Cui, P. Cheng, *Inorg. Chem. Front.* 1 (2014) 242–248.
- [64] T. Hu, Baohua Zheng, X. Wang, X. Hao, *CrystEngComm* 17 (2015) 9348–9356.
- [65] S. Goswami, G. Leitus, B.K. Tripuramallu, I. Goldberg, *Cryst. Growth Des.* 17(2017) 4393–4404.
- [66] G.-C. Liu, Y. Qu, X.-L. Wang, J.-W. Zhang, X.-M. Kan, N.-L. Chen, *Z. Anorg. Allg. Chem.* 640 (2014) 1696–1704.
- [67] X. Meng, H. Hou, G. Li, B. Ye, T. Ge, Y. Fan, Y. Zhu, H. Sakiyama, *J. Organomet. Chem.* 689 (2004) 1218–1229.
- [68] H. Sakiyama, R. Ito, H. Kumagai, K. Inoue, M. Sakamoto, Y. Nishida, M. Yamasaki, *Eur. J. Inorg. Chem.* (2001) 2027–2032.
- [69] O. Fabelo, J. Pasán, F. Lloret, M. Julve, C. Ruiz-Pérez, *Inorg. Chem.* 47 (2008) 3568–3576.
- [70] M.-L. Han, Wang, S.-C. Wang, Feng, D.-F. Feng, *Cryst. Res. Tech.* 49 (2014) 276–282.
- [71] J. Qin, Y. Jia, H. Li, B. Zhao, D. Wu, S. Zang, H. Hou, Y. Fan, Yaoting, *Inorg. Chem.* 53 (2014) 685–687.
- [72] M.-L. Han, Y.-P. Duan, D.-S. Li, G.-W. Xu, Y.-P. Wu, J. Zhao, *Dalton Trans.* 43 (2014) 17519–17527.
- [73] J.-H. Qin, H.-R. Wang, Q. Pan, S.-Q. Zang, H. Hou, Y. Fan, *Dalton Trans.* 44 (2015) 17639–17651.